AIMS Biophysics

ENRICHED
PUBLICATIONS

AIMS Biophysics

Aims and Scope

AIMS Biophysics is an international Open Access journal devoted to publishing peer-reviewed, high quality, original papers in the field of biophysics. We publish the following article types: original research articles, reviews, editorials, letters, and conference reports.

AIMS Biophysics welcomes, but not limited to, the papers from the following topics:

- Structural biology

- Biophysical technology

- Bioenergetics

- Membrane biophysics

- Cellular Biophysics

- Electrophysiology

- Neuro-Biophysics

- Biomechanics

- Systems biology

AIMS Biophysics

Managing Editor
Mr. Amit Prasad

AIMS Biophysics

(Volume No. 11, Issue No. 1, January - April 2024)

Contents

Exploring the role of preferential solvation in the stability of globular proteins through the study of ovalbumin interaction with organic additives

Tatyana Tretyakova1,*, Maya Makharadze1, Sopio Uchaneishvili1, Mikhael Shushanyan1 and Dimitri Khoshtariya1, 2

1 Laboratory of Biophysics, LEPL I. Beritashvili Center of Experimental Biomedicine, 0160 Tbilisi, Georgia

2Institute for Biophysics and Bionanosciences, Faculty of Exact and Natural Sciences, Ivane Javakhishvili Tbilisi State University, 0128 Tbilisi, Georgia

ABSTRACT

The impact of denaturing and stabilizing osmolytes on protein conformational dynamics has been extensively explored due to the significant contribution of protein solvation to the stability, function, malfunction and regulation of globular proteins. We studied the effect of two nonspecific organic molecules, urea, which is a conventional denaturant, and dimethyl sulfoxide (DMSO), which is a multilateral organic solvent, on the stability and conformational dynamics of a non-inhibitory serpin, ovalbumin (OVA). A differential scanning microcalorimetry (DSC) experimental series conducted in the phosphate buffer solutions containing 0–30 % of additives revealed the destabilizing impact of both urea and DMSO in a mild acidic media, manifested in the gradual decrease of thermal unfolding enthalpy and transition temperature. These findings differ from the results observed in our study of the mild alkaline DMSO buffered solutions of OVA, where the moderate stabilization of OVA was observed in presence of 5–10% of DMSO. However, the overall OVA interaction patterns with urea and DMSO are consistent with our previous findings on the stability and conformational flexibility of another model globular protein, α-chymotrypsin, in similar medium conditions. The obtained results could be explained by preferential solvation patterns. Positive preferential solvation of protein by urea in urea/water mixtures mainly weakens the hydrophobic interactions of the protein globule and eventually leads to the disruption of the tertiary structure within the whole range of urea concentrations. Alternatively, under certain experimental conditions in DMSO/water mixtures, positive preferential solvation by water molecules can be observed. We assume that the switch to the positive preferential solvation by DMSO, which is shown to have a soft maximum around 20–30% DMSO, could be shifted towards lower additive concentrations due to the intrinsic capability of ovalbumin OVA to convert into a heat-stable, yet flexible set of conformations that have increased the surface hydrophobicity, characteristic to molten-globule-like states.

Keywords: globular protein; protein stability; thermal unfolding; differential scanning calorimetry; ovalbumin; urea; dimethyl sulfoxide

Abbreviations: DSC: differential scanning calorimetry; OVA: ovalbumin; S-OVA: S-ovalbumin; DMSO: dimethyl sulfoxide; α-CT: α-chymotrypsin

1. Introduction

One of the major goals of both fundamental and applied biomedical sciences includes the profound

understanding of mechanisms governing various proteins' functions. Recent theoretical and experimental studies unveiled that protein function is essentially linked to its structure, stability and conformational flexibility, which, in turn, can be drastically altered by the crowded intracellular environment of proteins. According to the energy landscape theory of protein folding, general reaction coordinates of the multidimensional energy funnel of protein include both coupled and independent conformational and chemical transformations that are essential for protein folding and functional dynamics [1–4]. Thus, advanced knowledge and detailed understanding of protein structure and dynamics could provide new insights into the mechanisms governing protein function, as well as protein regulation, malfunction and degradation.

Our previous published works focused on the disclosure of intrinsic links between the stability, flexibility and function of globular proteins, such as α-chymotrypsin, carbxypeptidase A, cytochrome C, azurin and others, by altering their environment (solvent composition, immobilization etc). One of these works was devoted to understanding the impact of the same organic additives, urea and dimethyl sulfoxide (DMSO), on the conformational dynamics and enzymatic activity of α-chymotrypsin.

The goal of present work is to study the stability and conformational properties of model globular protein, hen egg albumin, or ovalbumin (OVA), from chicken egg whites in the presence of two nonspecific organic additives, urea and DMSO. The main conception of current manuscript emerged from the intention to investigate the peculiar action of DMSO on various model globular proteins.Ovalbumin is a major avian egg white protein with a well-studied structure, characteristic to the serpin superfamily of proteins. It is a glycoprotein consisting of a single 385 amino acid polypeptide chain glycosylated at Asn292 and cross-linked by one disulfide bond between Cys73–Cys120 [5,6]. Additionally, it should be mentioned that OVA has four more Cys residues with free sulfhydryl groups [5,6].

Previously referred to as the serine protease superfamily, serpins are numerous superfamily of proteins found in a vast majority of organisms, including animals, plants, fungi and viruses [7]. Most serpins are protease inhibitors, and are involved in processes such as coagulation (antithrombin), inflammation and immune processes (C1-inhibitor), among others. However, some of them, including ovalbumin, perform a non-inhibitory role, such as hormone transport (thyroxine-binding globulin) [8] and chaperone functions (heat shock serpin 47, myeloid and erythroid nuclear termination stage-specific protein (MENT)) [9,10].

Although possessing a similar amino acid composition and conformational resemblance, OVA is an atypical member of the serpin superfamily. It does not share an ability to inhibit serine proteases and little is known about its function so far [10,11]. A lack of inhibitory properties in OVA could derive from a difference in the part of the polypeptide chain that is homologous to the reactive center loop of inhibitory serpins and has an α-helical conformation [6]. Nevertheless, it is theorized that the presenceof a charged arginine residue within the active center drastically slows the loop insertion into the αsheet, further preventing any inhibitory function [6,12]. Presumably, OVA mainly has an amino acid storage function, though it could also be involved in the transport and storage of metal ions [13].

Another remarkable feature of OVA is an ability to irreversibly transform into a thermostable conformation, S-ovalbumin (S-OVA), upon storage [14]. The melting temperature of the S-OVA increases by approximately 8 °C compared to that of the native protein [15]. In vivo, the conversion process spontaneously occurs during egg storage as a consequence of a natural increase of pH level.

The rate of the conformational transfer is temperature and pH dependent [15]. Remarkably, although heat-stable S-OVA has a more compact structure and is more stable against thermal- or denaturant induced unfolding [13,14], it has a more hydrophobic surface and increased flexibility [6,12,16] compared to the native, heat-unstable conformer. In addition to egg whites, heat-stable ovalbumin is

found in egg yolks, then is transported into the amniotic fluid and subsequently absorbed by the embryonic organs [17]; it seems feasible that S-ovalbumin is required for the normal development of embryos [10,17].

The native ability of serpins to perform significant conformational changes is essential for their function. On the other hand, this ability is the very reason they are susceptible to misfolding and aggregation, leading to physiological disorders associated with serpin deficiencies, fatal accumulation of malfunctioning polymers and amyloid sheets formation [18], that eventually cause cell apoptosis and organ damage [19]. Considering the remarkable conformational flexibility, wide range of important functions and serpin misfolding related diseases [11,20], serpin family proteins have long been considered as a relevant research object of fundamental studies [5–10,21,22], as well as medical research [23,24] and bio-nanotechnology [25,26].

In the present work, we carried out a comparative study of the effect of urea, which is a conventional denaturant, and DMSO, which is a multilateral affecter, to explore the stability and conformational flexibility of OVA. DMSO is a dipolar organic solvent and is widely used in scientific research and medicine [27–29]. DMSO is reported to have multilateral action on protein stability and folding, exhibiting either stabilizing [29,30] or denaturizing [27,31] effects depending on experimental conditions. Additionally, it is used as a molecular chaperon [32,33], inhibitor [34,35] and activator [36]. However, its impact on OVA has not yet been sufficiently investigated.

2. Materials and methods
2.1. Differential scanning microcalorimetry
We applied differential scanning microcalorimetry (DSC) to measure the thermodynamic parameters of OVA thermal unfolding in the presence of a wide range of additives concentrations. Calorimetric measurements were carried out using a DASM-4 adiabatic scanning calorimeter (Biopribor, Russia) directly connected to a computer via a PCI-DAS1001 (Measurement Computing Corporation) interface unit. Further calorimetric data proceeding was carried out using the OriginLab software. Throughout all experiments, the heating and cooling rates were 1 K/min.

DSC is a very powerful experimental method for the investigation of the thermodynamic stability of globular proteins under the influence of various organic additives. It allows for the direct measurement of the biomolecule's enthalpy by plotting the partial heat capacity as a function of temperature. From the recorded DSC thermograms, the melting temperature T (melting peak x coordinate), transition enthalpy ΔH (melting peak area) and other thermodynamic parameters can be calculated [37,38].

If the protein thermal unfolding (melting) process follows a two state model, the heat capacity of the dissolved protein *Cp(prot)* can be determined at any temperature, according to the following equation [37,38]:

$$\Delta C_{p(app)} = C_{p(prot)} m_p - C_{p(solv)} \Delta m_s \tag{1}$$

where ΔCp(app) is the deviation of the protein sample's calorimetric curve from the baseline curve, Cp(prot) and Cp(solv) are the partial heat capacities of the protein and solvent, respectively, mp is the mass of the dissolved protein, and Δms is the mass of the replaced solvent. The calorimetric enthalpy ΔHcal of thermal melting having a single transition temperature, Tm, can be calculated using the following equation:

$$\Delta H_{cal} = \int_{T_1}^{T_2} C_p(T) dT \tag{2}$$

where T is the absolute temperature, and T1 and T2 are the temperatures of the initial and end point of the thermal melting peak, respectively.

Since the value of the calorimetric enthalpy ΔHcal is the area of the melting peak, it does not depend on the absolute value of the Cp(prot) (T). Consequently, determination of ΔHcal does not require the measurement of the absolute values of the partial heat capacities of both the protein and the solvent.

Thus, a zero-baseline-correction of the initial calorimetric curves can be made to simplify the data processing and to allow for a direct comparison of the calorimetric enthalpies of the protein in the presence of various mixed solvents.

All the calorimetric melting curves obtained throughout the experimental series (Figure 1) were baseline-corrected to avoid any errors derived from unknown parameters, such as Cp(solv) and Δms, and ΔHcal was calculated using Formula (2). An analysis of the thermograms provides reliable information on the reversibility and cooperativity of the protein unfolding process and allows for the detection of the transition to the molten-globule state, alongside the presence of unfolding intermediates, protein domains or aggregation, if available [37]. Comparison of the thermodynamic parameters of the protein under different environmental conditions (several denaturing/stabilizing additives at variable concentrations etc.) gives new insights into the fundamental aspects of the protein globule stability and flexibility [38,39].

2.2. Chemicals and experimental details

Highly purified albumin from hen egg white (OVA) (M = 42.7 kDa) was purchased from Sigma and used without further purification. DMSO was a product of Lugal (Ukraine) and contained 1% water as an impurity, which was considered to prepare any DMSO buffered solutions. Urea and all other chemicals were from Reakhim (Russia), of the highest purity available, and used as received. Phosphate buffer components were from Sigma. Doubly distilled water was used throughout all experiments.

The OVA samples for the DSC experiments were prepared by dissolving it in a 0.1 M phosphate buffer solution pH 6.1 at concentrations of 3 mg/ml, containing various concentrations of either urea or DMSO.

Since the addition of DMSO causes a concentration dependent increase in the pH of DMSO buffer mixtures, the buffer solutions with different DMSO concentrations were prepared by mixing solutions containing zero and maximal (30% DMSO v/v) concentration of DMSO, with the pH values being adjusted separately using concentrated citric acid.

3. Results and discussion

The thermal stability of OVA was studied in a mildly acidic media, namely 0.1 M phosphate buffer solutions containing no additive, 5, 10, 20 and 30% of either urea or DMSO. The initial DSC thermograms of the OVA at the heating rate of 1 K/min showed a single cooperative endothermic peak corresponding to a heat-unstable conformer of ovalbumin, while no peaks corresponding to S-ovalbumin were detected. Calorimetric parameters obtained from reference curves containing no additive in the solution were consistent with other published data obtained under similar conditions [12,40]. No protein refolding after denaturation was observed throughout the experimental series. Figures 1a and 1b show the temperature-dependent changes of the partial heat capacity of the OVA obtained in the presence of various urea and DMSO concentrations. The initial experimental curves were zero-baseline corrected and aligned. DSC experiments revealed a similar behavior of the thermodynamic parameters in the presence of urea and DMSO additives. Namely, in the whole range of buffered additive solutions, OVA exhibited gradual destabilization, manifested in a decrease of both the

denaturation temperature, Tm, and calorimetric enthalpy ΔHcal (i.e., the peak position gradually shifted towards lower temperatures and the peak area decreased monotonically with the increase of either additive concentration) (See Table 1 for details). However, it should be noted that within the concentration range between 0–20% of an additive the calorimetric enthalpies of OVA in DMSO solutions exceed that of the urea solutions, while the ΔHcal values for the solutions containing 30% DMSO dropped lower compared to the 30% urea solution. Urea is known to be a nonspecific denaturant, thereby increasing the flexibility of the protein globule and eventually causing destabilizing effects [39,41,42]; alternatively, since DMSO is a nonspecific affecter, it has been shown to exhibit either a stabilizing or destabilizing action, depending on the experimental conditions [27,29–31,43].

Thus, our results indicate that in the mildly acidic media (pH 6.1), DMSO acts as a conventional denaturant, causing destabilization of the OVA globule in the whole range of DMSO concentrations. These results are opposite to that acquired in our study of OVA within the mildly alkaline DMSO buffered solutions [44]. The thermodynamic parameters obtained from the thermal melting (unfolding) curves of OVA at pH 8 in the presence of similar DMSO concentrations indicate a notable increase of both, the melting temperature and the enthalpy, for the 5% DMSO solution. Moreover, in the presence of 10% DMSO (pH 8), the calorimetric enthalpy and the transition temperature are comparable to that of the reference solution with no DMSO added (Figure 2 and 3). However, a further increase of DMSO concentrations leads to a gradual decrease of both thermodynamic parameters. However, for the solutions containing 0–30% of urea, the calorimetric plots depict a gradual destabilization of the protein globule comparable to that of the pH 6.1 series, which means that both the melting temperature Tm and the calorimetric denaturation enthalpy ΔHcal decreased gradually within the whole range of urea concentrations. Thus, within the applied concentration range of additives, the experimental data indicate a similar denaturizing impact of urea at both an acidic and alkaline pH, and a diverse impact of DMSO at an alkaline pH, differing by the moderate stabilization of OVA in the presence of low concentrations of DMSO.
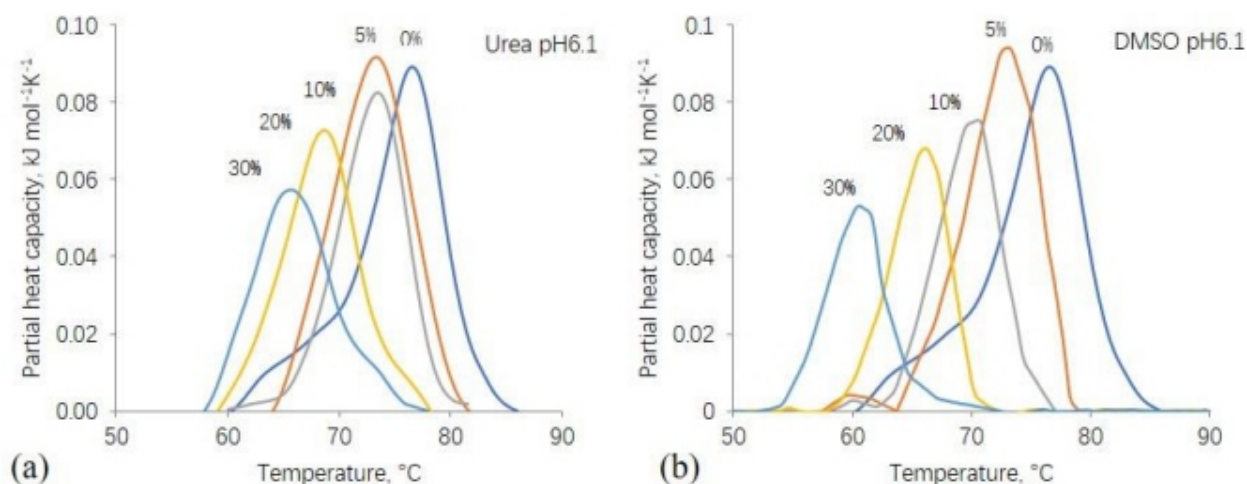

Figure 1. DSC curves for the OVA thermal unfolding in the presence of 0–30% urea (a) and DMSO (b) concentrations, 0.1 M phosphate buffer pH 6.1.

Table 1. Calorimetric enthalpy and melting temperature for the thermal unfolding of the OVA in the presence of 0–30% additive concentrations, 0.1 M phosphate buffer pH 6.1 and pH 8 [44].

Additive concentration, %	Urea, pH 6.1		DMSO, pH 6.1		Urea, pH 8 [44]		DMSO, pH 8 [44]	
	ΔH_{cal} (kJ/Mol)	T_m, °C	ΔH_{cal} (kJ/Mol)	T_m, °C	ΔH_{cal} (kJ/Mol)	T_m, °C	ΔH_{cal} (kJ/Mol)	T_m, °C
0	287	77	287	77	243	74	243	74
5	240	74	262	73	204	72	285	75
10	191	73	219	71	191	70	239	73
20	163	69	170	66	173	68	174	67
30	154	65	116	61	169	65	131	62
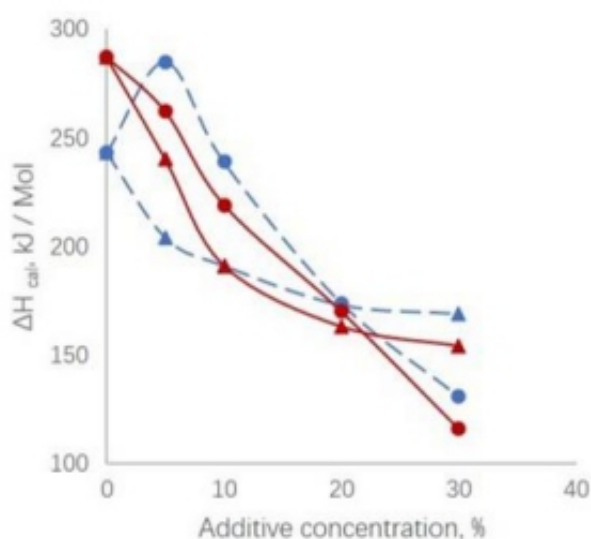
Figure 2. Dependencies of calorimetric enthalpies of thermally induced denaturation of ovalbumin on the DMSO concentration at pH 6.1 (red lines) compared with pH 8 (blue lines) [44]. Triangles represent urea and circles–DMSO.
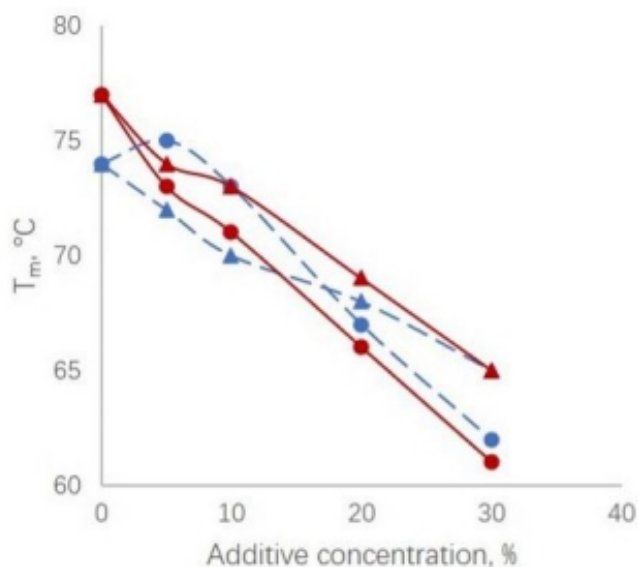
Figure 3. Dependencies of transition temperatures of thermally induced denaturation of ovalbumin on the DMSO concentration at pH 6.1 (red lines) compared with pH 8 (blue lines) [44]. Triangles represent urea and circles–DMSO.

The presented results are consistent with our previous findings on the impact of urea [39] and DMSO [43] on the stability and conformational flexibility of another model globular protein, αchymotrypsin (α-CT). These studies were also carried out in acidic and alkaline phosphate buffer solutions in presence of a wide range of urea (0-6M) and DMSO concentrations (0–70% vol.). Calorimetric parameters obtained for α-chymotrypsin displayed a similar behavior of the protein; namely, in alkaline DMSO solutions (pH 8.1), both the transition temperature Tm and calorimetric enthalpy of thermal unfolding ΔHcal increase in presence of low DMSO concentrations (5–30% vol.), thereby indicating protein globule stabilization with a soft maximum around 20% DMSO. A further increase of the DMSO concentration was followed by a gradual decrease of both thermodynamic parameters and resulted in the total destabilization of the protein in the presence of 70% DMSO. However, in acidic buffered solutions of DMSO (pH 2.6), as well as in both acidic and alkaline urea solutions, α-chymotrypsin was shown to undergo monotonous destabilization through the Tm within the whole range of additives concentrations (0–70%), while still retaining an enthalpic stabilization in acidic DMSO solutions [39,43].

It is noteworthy that while global stabilization of α-chymotrypsin exhibited a smooth maximum of protein stability around 20% DMSO, the enzymatic activity of α-chymotrypsin exhibited a monotonic decrease within the whole range of additive concentrations [43]. This effect can be explained by the different distribution of solvent-exposed hydrophobic amino acids within the active site and the surface of α-CT; thus, partially hydrophobic DMSO molecules can potentially cause local destabilization of the protein prior to the global destabilization of the entire globule. On the other hand, the relatively small area of the active site of α-chymotrypsin is characterized by an intrinsic flexibility, which is crucial for the substrate recognition and its further hydrolysis. Consequently, it is not expected to make a quantitatively significant enthalpic contribution into the global stability of the protein globule.

A computational study of Roy et al., which is consistent with a large number of experimental studies [45], has also reported a stabilizing effect of low concentrations of aqueous solutions of DMSO on lysozyme. It has been shown that conformational fluctuations of the protein globule are rather confined around 5–20% DMSO compared to the native state (0% DMSO), resulting in the formation of more compact protein conformations. However, in contrast with the functional kinetic study of chymotrypsin [43], the enzymatic activity of lysozyme was increased in presence of low DMSO concentrations. Unfortunately, in case of OVA, it is not possible to explore local destabilization patterns to compare with that of either the lysozyme or α-CT, because OVA is not capable of inhibiting serine proteases due to minor structural differences within the active site area [6,10–12] and no other active function of OVA is well described within the literature.

According to computational and experimental studies impact of urea and DMSO the on the stability of globular proteins can be explained by preferential solvation patterns [27,39,43–48]. Considering the nonspecific interaction of both additives with a protein globule, the either stabilizing or destabilizing effects occur due to multipoint weak interactions of the additive molecules with the protein amino acid residues and/or interfacial water. The positive preferential solvation of proteins by urea in urea/water mixtures mainly weakens hydrophobic interactions of the protein globule within the whole range of concentrations and eventually leads to the disruption of the protein tertiary structure [41,42,47,48]. However, in DMSO/water mixtures under certain experimental conditions, the positive preferential solvation by water molecules can be observed [45,46]. In the presence of low concentrations of DMSO,

, the latter can strengthen hydrogen bonds of interfacial water molecules and raise the compactness of the protein globule. This effect is common for a number of organic additives such as glycerol, TMAO and sugars that stabilize globular proteins, mainly via the confinement of water molecules in the protein hydration shell [47]. It is noteworthy that mainly hydrophobic protein DMSO interactions may provide a chaperone effect and protect some proteins from aggregation depending on the environmental conditions and intrinsic properties of the protein. As shown earlier, DMSO molecules primarily interact with the hydrophobic residues of proteins, which are mainly hidden inside the core of the native protein, but are largely presented on the surface of the molten globule-like conformations. In fact, our study of the thermal unfolding of α-chymotrypsin revealed a remarkable chaperone effect of DMSO. Although partial refolding of α-CT at pH 2.6 was observed even in the total absence of DMSO additives, the repetitive reversibility of the protein thermal unfolding only occurred in 20% DMSO solutions (pH 2.6). Namely, the refolding ability of α-CT was raised to 75%, as compared to 54% (0% DMSO), thereby displaying a multifold total repeatability for 24 hours [43].

Although the positive preferential solvation by water (thus, negative preferential solvation by DMSO) does equate to the total distancing of DMSO molecules from the protein interface, the further increase of DMSO concentration (20–30% DMSO or more) leads to the transition of preferential solvation in favor of DMSO, thereby causing a decrease of protein compactness, the reveal of a hydrophobic core and a drastic increase in the number of DMSO interactions with protein hydrophobic groups [45,46,48]. This leads to the destabilization of α-helices and eventually results in the total denaturation of the protein at higher DMSO concentrations [49]. The transition of the preferential solvation of OVA in buffered DMSO solutions is visualized in a rather noticeable drop of enthalpy when compared to a more gradual enthalpy decrease observed in presence of urea solutions at both pH values (Table 1). We assume that the soft maximum of DMSO/water preferential solvation pattern could be shifted towards the lower concentrations of the additive when compared to α-chymotrypsin due to the intrinsic ability of ovalbumin to perform an irreversible conversion to the specific thermo stable conformer, S-ovalbumin. Despite being more compact compared to the native form, S-OVA form has exceptionally flexible intermediate conformations with increased surface hydrophobicity, which, in general, is characteristic to partially unfolded molten-globule-like states [10–14,16,19,20].

Thus, the destabilization of OVA via direct hydrophobic interactions with DMSO molecules, could start in the presence of lower DMSO concentrations. According to a comparative computational study of solvation patterns of the conventional denaturant urea with the conventional stabilizer TMAO in water-additive mixtures, in presence of TMAO, an extra hydration shell is observed near hydrophobic groups; alternatively, in urea solutions, the urea urea and water-water association is found to be more favored than the urea-water association [50]. The addition of TMAO displayed an increase in the strength and the hydrogen bond lifetime within the solution. Moreover, the computations revealed that near the interface of amino acids (i.e., near the protein surface), water molecules are preferentially favored over the other co-solvents [50]. Thus, the stabilizing effect of TMAO occurs due to an increase of the hydration shell around the protein, especially around the hydrophobic groups of the biomolecules, and due to strengthening the hydrogen bond network of the solution. However, the destabilizing effect of urea manifests itself in a disruption of the protective interfacial water layers and decreasing the overall interaction between the amino acid residues and the solvent molecules.

Considering that DMSO and TMAO are both small dipolar compounds containing hydrophobic methyl groups and an oxygen atom capable of forming hydrogen bonds with water molecules (within the S=O and N–O groups, respectively), it is safe to assume that they could also share some similarities in their mechanisms of protein stabilization. A combined experimental and theoretical study of the interaction of TMAO and DMSO with a K-peptide, which is a fragment of hen egg white lysozyme [51], confirmed

that both TMAO and DMSO prefer interactions with water molecules in diluted solutions. However, in presence of higher additive concentrations, the amount of water-TMAO interactions gradually increase and lead to a stronger TMAO hydration, while the hydration of DMSO weakens, which gives rise to the differences in the protein-additive interaction.4. ConclusionsWe used DSC to study the impact of two nonspecific organic compounds, urea, which is a conventional denaturant, and DMSO, which is a multilateral organic solvent, on the conformational dynamics of OVA. Experimental results obtained in phosphate buffer solutions containing 0–30 % of additives revealed the destabilizing impact of both urea and DMSO in a mildly acidic media, as manifested in the gradual decrease of the thermal unfolding enthalpy and the transition temperature.

These results substantially differ from the calorimetric parameters observed in our study of OVA within mildly alkaline buffered solutions of DMSO, where the moderate stabilization of OVA was observed in presence 5–10% of DMSO. However, the overall pattern of the OVA interaction with urea and DMSO is consistent with our previous findings on the stability and conformational flexibility of another model globular protein, α-chymotrypsin, in similar medium conditions. Thus, our findings on the OVA stability could also be explained by preferential solvation patterns. The positive preferential solvation of a protein by urea in urea/water mixtures mainly weakens the hydrophobic interactions of the protein globule and eventually leads to the disruption of the tertiary structure within the whole range of urea concentrations. However, in DMSO/water mixtures, the positive preferential solvation by water molecules can be observed under certain experimental conditions. Low concentrations of DMSO remotely strengthen the bond water networks of the protein, thereby protecting it from unfolding, whereas a subsequent increase of DMSO concentration leads to a switch of preferential solvation and the gradual destabilization of the protein.

Use of AI tools declaration

The authors declare they have not used Artificial Intelligence (AI) tools in the creation of this article.

Conflict of interest

The authors declare no conflict of interest.

References

1. Onuchic JN, Nymeyer H, García AE, et al. (2000) The energy landscape theory of protein folding: insights into folding mechanisms and scenarios. Adv Protein Chem 53: 87–152. https://doi.org/10.1016/S0065-3233(00)53003-4

2. Whitford PC, Onuchic JN (2015) What protein folding teaches us about biological function and molecular machines. Curr Opin Struct Biol 30: 57–62. https://doi.org/10.1016/j.sbi.2014.12.003

3. Schug A, Onuchic JN (2010) From protein folding to protein function and biomolecular binding by energy landscape theory. Curr Opin Pharmacol 10: 709–714. https://doi.org/10.1016/j.sbi.2014.12.003

4. Warshel A, Parson W (2001) Dynamics of biochemical and biophysical reactions: insight from computer simulations. Q Rev Biophys 34: 563–679. https://doi.org/10.1017/S0033583501003730

5. Stein PE, Leslie AGW, Finch JT, et al. (1991) Crystal structure of uncleaved ovalbumin at l.95 aresolution. J Mol Biol 221: 941–959. https://doi.org/10.1016/0022-2836(91)80185-W

6. Stein PE, Huntington JA (2001) Structure and properties of ovalbumin. *J Chromat B* 756: 189–198. https://doi.org/10.1016/S0378-4347(01)00108-6

7. Law RH, Zhang Q, McGowan S, et al. (2006) An overview of the serpin superfamily. *Genome Biol* 7: 216. https://doi.org/10.1186/gb-2006-7-5-216

8. Carrell RW, Read RJ (2017) How serpins transport hormones and regulate their release. *Semin Cell Dev Biol* 62: 133–141. https://doi.org/10.1016/j.semcdb.2016.12.007

9. Bose D, Chakrabarti A (2017) Substrate specificity in the context of molecular chaperones. *IUBMB Life* 69: 647–659. https://doi.org/10.1002/iub.1656

10. Shinohara H, Iwasaki T, Miyazaki Y, et al. (2005) Thermostabilized ovalbumin that occurs naturally during development accumulates in embryonic tissues. *Biochim Biophys Acta* 1723: 106–113. https://doi.org/10.1016/j.bbagen.2005.02.016

11. Da Silva M, Beauclercq S, Harichaux G, et al. (2015) The family secrets of avian egg-specific ovalbumin and its related proteins Y and X. *Biol Reprod* 93: 71. https://doi.org/10.1095/biolreprod.115.130856

12. Huntington JA, Patston PA, Gettins PG (1995) S-ovalbumin, an ovalbumin conformer with properties analogous to those of loop-inserted serpins. *Protein Sci* 4: 613–621. https://doi.org/10.1002/pro.5560040403

13. Castellano AC, Barteri M, Bianconi A, et al. (1996) Conformational changes involved in the switch from ovalbumin to S-ovalbumin. *Z Naturforsch C J Biosci* 51: 379–385. https://doi.org/10.1515/znc-1996-5-615

14. Paolinelli C, Barteri M, Boffi F, et al. (1997) Structural differences of ovalbumin and S-ovalbumin revealed by denaturing conditions. *Z Naturforsch C J Biosci* 52: 645–653. https://doi.org/10.1515/znc-1997-9-1012

15. Hammershøj M, Larsen LB, Andersen A B, et al. (2002) Storage of shell eggs influences the albumen gelling properties. *LWT-Food Sci Technol* 35: 62–69. https://doi.org/10.1006/fstl.2001.0811

16. Nakamura R, Ishimaru M (1981) Changes in the shape and surface hydrophobicity of ovalbumin during its transformation to S-ovalbumin. *Agr Biol Chem* 45: 2775–2780. https://doi.org/10.1080/00021369.1981.10864966

17. Sugimoto Y, Sanuki S, Ohsako S, et al. (1999) Ovalbumin in developing chicken eggs migrates from egg white to embryonic organs while changing its conformation and thermal stability. *J Biol Chem* 274: 11030–11037. https://doi.org/10.1074/jbc.274.16.11030

18. Tufail S, Sherwani MA, Shoaib S, et al. (2018) Ovalbumin self-assembles into amyloid nanosheets that elicit immune responses and facilitate sustained drug release. *J Biol Chem* 293: 11310–11324. https://doi.org/10.1074/jbc.RA118.002550

19. Khan MS, Singh P, Azhar A, et al. (2011) Serpin inhibition mechanism: a delicate balance between native metastable state and polymerization. *J Amino Acids* 2011: 606797. https://doi.org/10.4061/2011/606797

20. Bhattacharya M, Mukhopadhyay S (2012) Structural and dynamical insights into the molten globule form of ovalbumin. *J Phys Chem B* 116: 520–531. https://doi.org/10.1021/jp208416d21. Huntington JA (2011) Serpin structure, function and dysfunction. *J Thromb Haemost* 9: 26–34. https://doi.org/10.1111/j.1538-7836.2011.04360.x

22. Akazawa T, Ogawa M, Hayakawa S, et al. (2018) Structural change of ovalbumin-related protein X by alkali treatment. *Poult Sci* 97: 1730–1737. https://doi.org/10.3382/ps/pey024

23. Tanaka N, Morimoto Y, Noguchi Y, et al. (2011) The mechanism of fibril formation of a non inhibitory serpin ovalbumin revealed by the identification of amyloidogenic core regions. *J Biol Chem* 286: 5884–5894. https://doi.org/10.1074/jbc.M110.176396

24. Jin H, Li P, Jin Y, et al. (2021) Effect of sodium tripolyphosphate on the interaction and aggregation behavior of ovalbumin-lysozyme complex. *Food Chem* 352: 129457. https://doi.org/10.1016/j.foodchem.2021.129457

25. Zhou J, Geng S, Wang Q, et al. (2020) Ovalbumin-modified nanoparticles increase the tumor accumulation by a tumor microenvironment-mediated "giant". *J Mater Chem B* 8: 7528–7538. https://doi.org/10.1039/D0TB00542H

26. Kavitha K, Palaniappan L (2022) FTIR study of synthesized ovalbumin nanoparticles. *Anal Biochem* 636: 114456. https://doi.org/10.1016/j.ab.2021.114456

27. Magsumov T, Fatkhutdinova A, Mukhametzyanov T, et al. (2019) The effect of dimethyl sulfoxide on the lysozyme unfolding kinetics, thermodynamics, and mechanism. *Biomolecules* 9: 547. https://doi.org/10.3390/biom9100547

28. Karim M, Boikess, RS, Schwartz RA, et al. (2023) Dimethyl sulfoxide (DMSO): a solvent that may solve selected cutaneous clinical challenges. *Arch Dermatol Res* 315: 1465–1472.https://doi.org/10.1007/s00403-022-02494-1

29. Oh KI, Baiz CR (2018) Crowding stabilizes DMSO-water hydrogen-bonding interactions. *J Phys Chem B* 122: 5984–5990. https://doi.org/10.1021/acs.jpcb.8b02739

30. Nandi S, Parui S, Halder R, et al. (2018) Interaction of proteins with ionic liquid, alcohol and DMSO and in situ generation of gold nano-clusters in a cell. *Biophys Rev* 10: 757–768. https://doi.org/10.1007/s12551-017-0331-1

31. Krylov AV, Pfeil W, Lisdat F (2004) Denaturation and renaturation of cytochrome c immobilized on gold electrodes in DMSO-containing buffers. *J Electroanal Chem* 569: 225–231. https://doi.org/10.1016/j.jelechem.2004.03.005

32. Kim SH, Yan YB, Zhou HM (2006) Role of osmolytes as chemical chaperones during the refolding of aminoacylase. *Biochem Cell Biol* 84: 30–38. https://doi.org/10.1139/o05-148

33. Ou WB, Park YD, Zhou HM (2002) Effect of osmolytes as folding aids on creatine kinase refolding pathway. *Int J Biochem Cell Biol* 34: 136–147. https://doi.org/10.1016/S1357-2725(01)00113-3

34. Kumar A, Darreh-Shori T (2017) DMSO: A mixed-competitive inhibitor of human acetylcholinesterase. *ACS Chem Neurosci* 8: 2618–2625. https://doi.org/10.1021/acschemneuro.7b00344

35. Murray KA, Gibson MI (2022) Chemical approaches to cryopreservation. *Nat Rev Chem* 6: 579–593. https://doi.org/10.1038/s41570-022-00407-4

36. Almarsson O, Klibanov AM (1996) Remarkable activation of enzymes in nonaqueous media by denaturing organic cosolvents. *Biotechnol Bioeng* 49: 87–92. https://doi.org/10.1002/(SICI)1097-0290(19960105)49:1<87::AID-BIT11>3.0.CO;2-8

37. Privalov PL, Gill SG (1988) Stability of protein structure and hydrophobic interaction. *Adv Protein Chem* 39: 191–234. https://doi.org/10.1016/S0065-3233(08)60377-0

38. Kim PS, Baldwin RL (1990) Intermediates in the folding reactions of small proteins. *Annu Rev Biochem* 59: 631–660. https://doi.org/10.1146/annurev.bi.59.070190.003215

39. Khoshtariya D, Shushanian M, Sujashvili R, et al. (2003) Enzymatic activity of α-chymotrypsin in the urea-induced molten-globule-like state: a combined kinetic/thermodynamic study. *J Biol Phys Chem* 3: 2–10.

40. Yamasaki M, Takahashi N, Hirose M (2003) Crystal structure of S-ovalbumin as a non-loopinserted thermostabilized serpin form. *J Biol Chem* 278: 35524–35530. https://doi.org/10.1074/jbc.M305926200

41. Timasheff SN, Xie G (2003) Preferential interactions of urea with lysozyme and their linkage to protein denaturation. *Biophys Chem* 105: 421–448. https://doi.org/10.1016/S0301-4622(03)00106-6

42. Nnyigide OS, Lee SG, Hyun K (2018) Exploring the differences and similarities between urea and thermally driven denaturation of bovine serum albumin: intermolecular forces and solvation preferences. J Mol Model 24: 75. https://doi.org/10.1007/s00894-018-3622-y

43. Tretyakova T, Shushanyan M, Partskhaladze T, et al. (2013) Simplicity within the complexity: Bilateral impact of DMSO on the functional and unfolding patterns of α-chymotrypsin. Biophys Chem 175–176: 17–27. https://doi.org/10.1016/j.bpc.2013.02.006

44. Tretyakova T, Makharadze M, Uchaneishvili S, et al. (2020) Impact of small organic molecules on the stability and conformational flexibility of globular proteins, Proceedings of International Conference on Life Sciences, Engineering and Technolog.

45. Roy S, Jana B, Bagchi B (2012) Dimethyl sulfoxide induced structural transformations and non monotonic concentration dependence of conformational fluctuation around active site of lysozyme. J Chem Phys 136: 115103. https://doi.org/10.1063/1.3694268

46. Arakawa T, Kita Y, Timasheff SN (2007) Protein precipitation and denaturation by dimethyl sulfoxide. Biophys Chem 131: 62–70. https://doi.org/10.1016/j.bpc.2007.09.004

47. Auton A, Bolen DW, Rösgen J (2008) Structural thermodynamics of protein preferential solvation: Osmolyte solvation of proteins, aminoacids, and peptides. Proteins 73: 802–813. https://doi.org/10.1002/prot.22103

48. Jaganade T, Chattopadhyay A, Raghunathan S, et al. (2020) Urea-water solvation of protein side chain models. J Mol Liq 311: 113191. https://doi.org/10.1016/j.molliq.2020.113191

49. Batista ANL, Batista JrJM, Bolzani VS, et al. (2013) Selective DMSO-induced conformational changes in proteins from Raman optical activity. Phys Chem Chem Phys 15: 20147–20152. https://doi.org/10.1039/C3CP53525H

50. Dilip HN, Chakraborty D (2019) Effect of cosolvents in the preferential binding affinity of water in aqueous solutions of amino acids and amides. J Mol Liq 300: 112375. https://doi.org/10.1016/j.molliq.2019.112375

51. Godlewska J, Cieśla B, Wawer J, et al. (2022) DMSO and TMAO-differences in interactions in aqueous solutions of the K-peptide. Int J Mol Sci 23: 1872. https://doi.org/10.3390/ijms23031872

Natural bond orbital analysis of dication magnesium complexes [Mg(H2O)6]2+ and [[Mg(H2O)6](H2O)n] 2+; n=1-4

Ganesh Prasad Tiwari1, Santosh Adhikari1, Hari Prasad Lamichhane2 and Dinesh Kumar Chaudhary1,2,*

1 Department of Physics, Amrit Campus, Tribhuvan University, Kathmandu 44600, Nepal

2 Central Department of Physics, Tribhuvan University, Kirtipur, Kathmandu 44618, Nepal

ABSTRACT

The metal ion is ubiquitous in the human body and is essential to biochemical reactions. The study of the metal ion complexes and their charge transfer nature will be fruitful for drug design and may be beneficial for the extension of the field. In this regard, investigations into charge transport properties from ligands to metal ion complexes and their stability are crucial in the medical field. In this work, the DFT technique has been applied to analyze the delocalization of electrons from the water ligands to a core metal ion. At the B3LYP level of approximation, natural bond orbital (NBO) analysis was performed for the first five distinct complexes [Mg(H2O)6]2+ and [[Mg(H2O)6](H2O)n]2+; n = 1-4. All these complexes were optimized and examined with the higher basis set 6-311++G(d, p). In the complex [Mg(H2O)6]2+, the amount of natural charge transport from ligands towards the metal ion was 0.179e, and the greatest stabilization energy was observed to be 22.67 kcal/mol. The donation of the p orbitals in the hybrid orbitals was increased while approaching the oxygen atoms of H2O ligands in the 1st coordination sphere with the magnesium ions. The presence of water ligands within the 2nd coordination sphere increased natural charge transfer and decreased the stabilizing energy of the complexes. This may be due to the ligand-metal interactions.

Keywords: DFT; B3LYP; delocalization; NBO; Ligand; dication

1. Introduction

Dication magnesium complexes have a unique place in chemistry and biochemistry due to their diverse structural arrangements and applications in numerous fields. Magnesium is very crucial for living beings. For example, about 300 metabolic activities and 800 proteins require this metal to function in our body. This metal is also necessary for DNA [1,2], RNA [3,4], antioxidant glutathione production [5], energy generation, oxidative phosphorylation, and glycolysis among other elements, helps the anatomical formation of bone, with exterior layers assisting in the maintenance of blood magnesium levels [6], while magnesium shortage has been associated with decreased bone mass [7,8]. In plants, Chlorophyll, a magnesium coordination molecule, is required for plant life (Photosynthesis) and the survival of life on Earth [9,10]. Magnesium also participates in active Ca and K ion transport across cell membranes, which are required for nerve impulse transmission, muscle contraction, and a regular heart rhythm [11,12].

Computational chemistry has recently acquired popularity among scholars and researchers as a method of addressing real-world challenges in chemical, pharmaceutical, biotechnology, and material science [13]. By Bock et al., the stereochemistry of ligand binding by bivalent magnesium metal was

effectively analyzed, as was how likely these ligands are to be water [14]. Ab initio molecular orbital (MO) calculation of M2+(H2O)n complexes having central alkaline earth metal ion with varying water ligands from one to six at RHF and MP2 level with basis set 6-31+G was investigated by Glendening et al. [15]. The alkaline-earth metal ions M2+(H2O)n, n = 5-7 (M = Mg, Ca, Sr, and Ba) hydration energies and geometries were determined by Rodriguez-Cruz et al. [16] using the DFT-B3LYP method. According to Pavlov et al. [17], charge transfer between the ligands and the metal lowers the interaction energy of the complex [Mg(H2O)n] 2+ between M···H2O as the number of ligands rises in the 2nd coordination sphere. By employing the kinetic energy release measurement method, Bruzzi et al. [18] investigated the binding energies of complexes [Mg(NH3)n]2+, [Ca(NH3)n]2+, and [Sr(NH3)n]2+for n = 4–20, and these results are supported by DFT calculations. These desired impacts have provided new insights into the trustworthiness of computational methodologies.
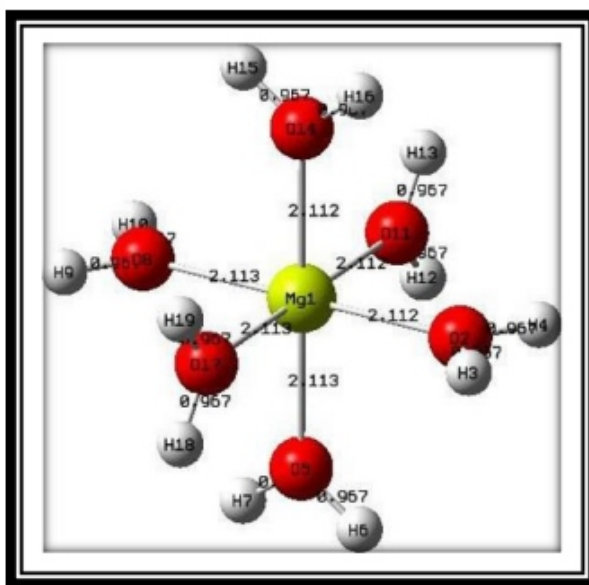
Figure 1. Structural representation of the octahedral magnesium complex [Mg(H2O)6]2+showing bond lengths.

Several preceding studies reveal the focus on the coordinative behavior of metal ions however, the natural bond orbital analysis of metal complexes by using the DFT-B3LYP approach with varying numbers of ligands in 2nd coordination sphere is yet to be studied. The charge transfer from surrounding ligands to a central metal ion and vice versa affects its geometry and other physical features of complexes. Two charge transfer mechanisms, Mulliken and natural, are explained by population analysis. NBO analysis provides a solid framework for researching charge transfer and conjugative interactions in atoms and molecules. The second-order perturbation hypothesis leads to the availability of some electron donor orbitals, acceptor orbitals, and association stabilization energies [19]. The system conjugation increases with increasing *E(2)* value and electron donor interaction. When electron density delocalizes between occupied Lewis type (bond or lone pair) and nominally vacant non-Lewis type (antibonding or Rydberg) NBO orbitals, a stable donor-acceptor interaction is ensured [17]. The natural bond orbital study of magnesium compounds using the DFT-B3LYP approach with varying quantities of ligands in 2nd coordination sphere remains unexplored. This work reports the study of natural transfer properties in the coordination complex [Mg(H2O)6] 2+. Figure 1 illustrates the optimized structural representation of complex [Mg(H2O)6]2+ that displays bond lengths. The central metal ion is attached to identical six water ligands, forming an octahedral structure.

The distance between Mg and O is 2.112 Å, while the distance between O and H is 0.967Å. The remaining four complexes were created by gradually expanding the number of water molecules within 2nd coordination sphere from one to four. Natural charge transfer behavior of the different complexes was then compared. This study of magnesium complexes will shed light on the charge transfer behavior of metal ions. The analysis of these complexes will be beneficial for medicinal design and could aid in the development of new drugs.

2. Materials and methods

The quantum computations in this extensive analysis of metal complexes were accomplished with the Gaussian 16 program packages [20]. Gaussian inputs of magnesium ion compounds were generated, and outputs were displayed using GaussView 6 [21]. The structural geometrics of complexes were firstly optimized utilizing various basis sets with B3LYP functional, which combines Becke's gradient-correlated exchange functional (B3) [22] and Lee-Yang-Parr (LYP) [23]. These inputs were acquired by retaining the ligands in a quasi-octahedral structure. There was no symmetry limitation enforced, and the C1 point group symmetry was used for optimization. Frequency estimations were carried out during the geometry optimization process, and global minima were validated. Every calculation was carried out by applying 6-311++G(d,p) basis set and B3LYP functional. NBOs provide precise details on the type of electronic conjugation occurring between molecular bonds. In metal complexes, the delocalization of electrons results once the hybridized orbitals of water molecules and metal ions coincides. NBO evaluation is a strong approach for determining this electron delocalization. NBOs strongly support the assumption that localized bonds and lone pairs are the essential building blocks of molecular structure, hence it is feasible to understand ab initio wave functions in perspective of Lewis structure theories by effectively converting them toNBO form. The NBO technique was utilized to study how the non-bonding pairs of oxygen atoms in the water decreased their native charge densities. NBO analysis is performed by looking at allconceivable interactions between 'full' (donor) Lewis-type NBOs and 'empty' (acceptor) non-Lewis NBOs and evaluating their energetic significance using second-order perturbation theory. Since these exchanges result in the transfer of occupancy from the idealized Lewis structure's localized NBOs into the unoccupied non-Lewis orbitals (and hence deviations from the idealized Lewis structure description), they are termed to as "delocalization" corrections to the zeroth-order natural Lewis structure [23]. This work presents the outcomes of a second-order perturbation theory investigation of the Fock matrix within the NBO of the complexes. The delocalization-related stabilizing energy $E(2)$ for each donating NBO (i) and receiver NBO (j) is determined as

$$E^{(2)} = q_i \frac{<i|\hat{F}|j>}{\epsilon_i - \epsilon_j}$$

Where q_i stands for orbital occupancy of a donor, E_i, E_j represents orbital energies, and F(i,j) for the off-diagonal NBO Fock matrix component [24]. Higher value of stabilization energy $E(2)$ denotes powerful interaction between acceptors and donors [25].

3. Results and discussion
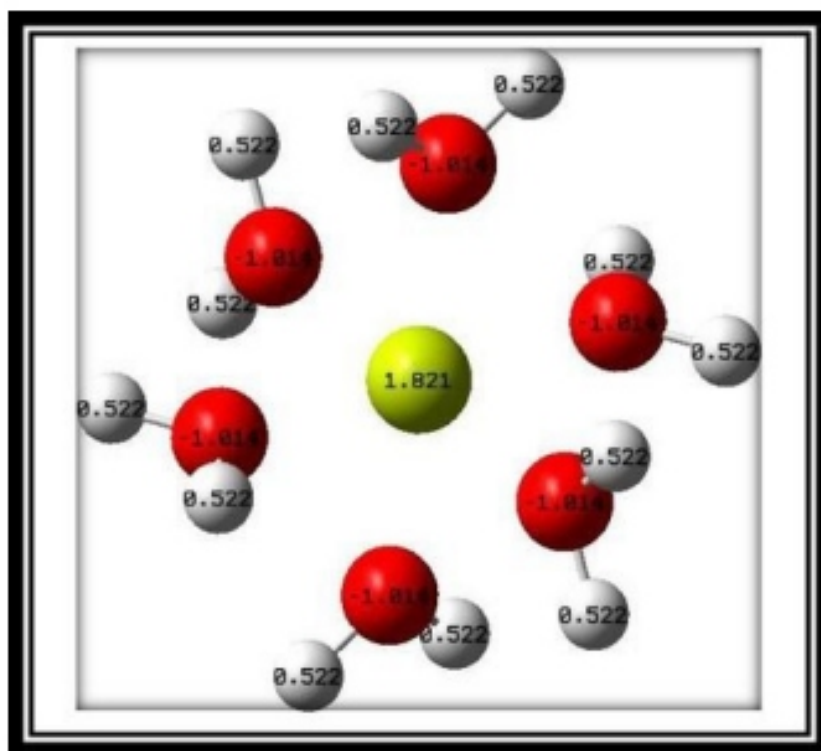
Figure 2. Natural charges on constituent atoms in the complex [Mg(H2O)6]2+.

Table 1. Natural charges on the central metal ion MgQ and ligands to metal chargetransfer ΔQ in the complexes [[Mg(H2O)6](H2O)n]2+; n = 0-4.

Complex	$Mg^Q(e)$	$\Delta Q(e)$
$[Mg(H_2O)_6]^{2+}$	1.821	0.179
$[[Mg(H_2O)_6](H_2O)]^{2+}$	1.820	0.180
$[[Mg(H_2O)_6](H_2O)_2]^{2+}$	1.819	0.181
$[[Mg(H_2O)_6](H_2O)_3]^{2+}$	1.818	0.182
$[[Mg(H_2O)_6](H_2O)_4]^{2+}$	1.817	0.183

The natural charges on the central metal ion Mg2+ and charge transfer in the complexes [[Mg(H2O)6](H2O)n]2+; n = 0-4 are demonstrated in Table 1. The charge transfer takes place in all complexes. The NBO partial charge on metal ions does not widely vary when the number of moleculeswithin the 2nd coordination sphere is increased, but there are modest increases, as shown in Table 1. Figure 2 depicts the octahedral structural representation of complex [Mg(H2O)6]2+ with natural charges on constituent atoms. This central metal ion is surrounded by six identical water molecules in the 1stcoordination sphere. The total charge constituent in the whole complex equals +2e. Figure 3(a) showsthe representation of the complex when one water ligand is added to its 2nd coordination sphere. Likewise, Figure 3(b), Figure 3(c), and Figure 3(d) represent the figurative representatives of complexes after the addition of two, three, and four water ligands to their 2nd coordination sphere, respectively. The total electron density of the [Mg(H2O)6]2+ is used to express the overall effectiveness of the natural Lewis structure analysis as a percentage. Table 2 demonstrates the importance of valance non-Lewis orbitals in comparison to extra-valence electron shells in modest

deviations from a confined Lewis structure model.
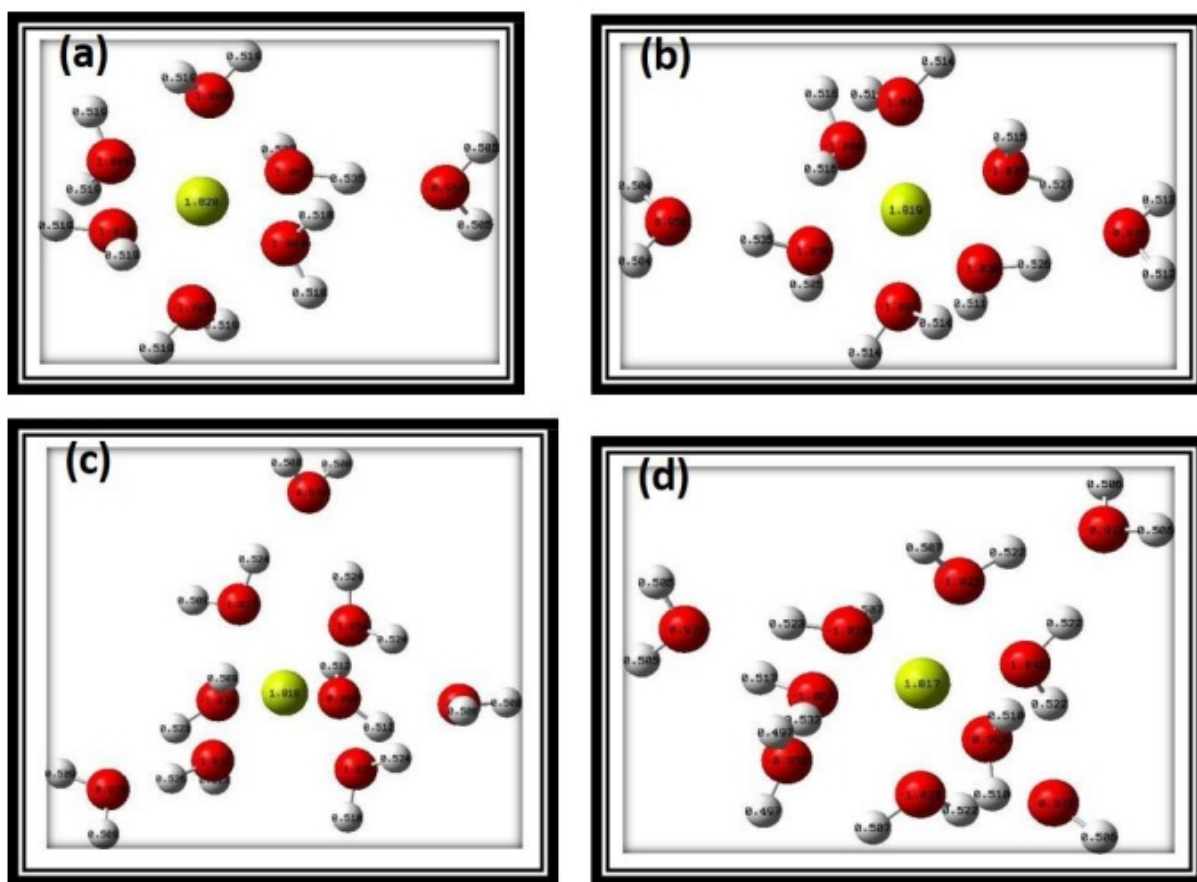
Figure 3. The natural charges on constituent atoms in the complex (a) [[Mg(H2O)6](H2O)]2+, (b) [[Mg(H2O)6](H2O)2]2+, (c) [[Mg(H2O)6](H2O)3]2+, and (d) [[Mg(H2O)6](H2O)4]2+ with extension of one to four ligands in the 2nd coordination sphere respectively.

Table 2. Separation of Lewis and non-Lewis occupancies within complex [Mg(H2O)6]2+into core, valence, and Rydberg shell components.

Orbitals	Occupancy
Core	21.99748 (99.989% of 22)
Valence Lewis	47.77540 (99.532% of 48)
Total Lewis	69.77288 (99.676% of 70)
Valence non-Lewis	0.18649 (0.266% of 70)
Rydberg non-Lewis	0.04063 (0.058% of 70)
Total non-Lewis	0.22712 (0.324% of 70)

The electron delocalization through lone pairs of oxygen to iron orbitals was evaluated. The table below shows the two most powerful interactions. The interchange of non-bonding pairs of oxygen with metal n^* orbitals is determined to be greatest in the instance of a complex [Mg(H2O)6]2+. The greatest interaction in the complex is likewise demonstrated to be between metal orbitals and virtual orbitals.

Table 3. Result of second-order perturbation theory evaluation of Fock matrix within NBO of complex [Mg(H2O)6]2+.

Donor NBOs	Occupancy (e)	Hybrid (%)	Acceptor NBOs	Occupancy (e)	Hybrid (%)	$E^{(2)}$ (kcal/mol)
LP O (2)	1.96849	$s47.65p52.34$	LP* Mg	0.17178	$s100$	22.67
LP O (5)	1.96853	$s47.66p52.34$	LP* Mg	0.17178	$s100$	22.63
LP O (8)	1.96853	$s47.65p52.34$	LP* Mg	0.17178	$s100$	22.63
LP O (11)	1.96851	$s47.66p52.34$	LP* Mg	0.17178	$s100$	22.66
LP O (14)	1.96849	$s47.65p52.34$	LP* Mg	0.17178	$s100$	22.67
LP O (17)	1.96854	$s47.66p52.34$	LP* Mg	0.17178	$s100$	22.62

From Table 3, it is seen that delocalization of oxygen lone pairs to $n*$ orbitals of Mg2+ occurred in the stronger interactions of LP O (2) and LP O (14) with LP*Mg with occupancy of 0.17178e stabilizes [Mg(H2O)6]2+ complex by 22.67 kcal/mol. These stabilization energies of complexes are balanced by the remaining stabilization energies of complexes. This analysis reveals that, on the donor orbital side, the p orbital contributes more than the s orbital, whereas the d orbital does not contribute.

On the acceptor side, the contribution of the p and d orbitals was negligible in comparison to the s orbital for the maximum stabilization energy. In a few cases of acceptor orbitals, the contribution of the p orbital and d orbital is also seen. The greatest stabilization energy of complex [Mg(H2O)6]2+ is less than that of the complex [Zn(H2O)6]2+ as reported by Pokharel et al. [26].The NBO partial charge on the metal ions does not change much on adding the number of ligands within the 2nd coordination sphere. It displays some findings from an investigation into the Fock matrix within the NBO of complexes by utilizing second-order perturbation analysis. Only the interaction resulting from the delocalization of the electrons from the oxygen lone pairs of ligands in the 1st coordination sphere to the $n*$ orbitals of Mg2+ was obtained to have stabilization energies of more than 5 kcal/mol in all circumstances. As a result, these tables only include the most powerful interactions. The powerful interaction among the associated interactions is one in which electrons from non-binding pairs of O (2) are delocalized to the LP Mg with occupancy 0.17343e, as shown in Table 4. This is the interaction when one water ligand is attached within the 2nd coordination sphere of a complex [Mg(H2O)6]2+. As shown by the preceding result, the bond between magnesium and oxygen has been shortened compared to that of the complex [Mg(H2O)6]2+ because of the presence of one water ligand in the 2nd coordination sphere.

Table 4. Result of second-order perturbation theory evaluation of matrix within NBO of the complex [[Mg(H2O)6](H2O)]2+.

Donor NBOs	Occupancy (e)	Hybrid (%)	Acceptor NBOs	Occupancy (e)	Hybrid (%)	$E^{(2)}$ (kcal/mol)
LP O (2)	1.96238	$s43.80p56.20$	LP* Mg	0.17343	$s100$	25.47
LP O (5)	1.96938	$s47.66p52.34$	LP* Mg	0.17343	$s100$	22.38
LP O (8)	1.96955	$s47.65p52.35$	LP* Mg	0.17343	$s100$	22.06
LP O (11)	1.96874	$s46.67p53.32$	LP* Mg	0.17343	$s100$	22.51

Donor NBOs	Occupancy (e)	Hybrid (%)	Acceptor NBOs	Occupancy (e)	Hybrid (%)	$E^{(2)}$ (kcal/mol)
LP O (14)	1.96938	s47.66p52.34	LP* Mg	0.17343	s100	22.37
LP O (17)	1.96967	s47.74p52.25	LP* Mg	0.17343	s100	22.15

Table 5. Result of second-order perturbation theory evaluation of Fock matrix within NBO of the complex [[Mg(H2O)6](H2O)2]2+.

Donor NBOs	Occupancy (e)	Hybrid (%)	Acceptor NBOs	Occupancy (e)	Hybrid (%)	$E^{(2)}$ (kcal/mol)
LP O (2)	1.96371	s44.71p55.79	LP* Mg	0.17413	s99.99p0.01	24.64
LP O (5)	1.97016	s46.32p53.67	LP* Mg	0.17413	s99.99p0.01	24.71
LP O (8)	1.96726	s44.71p55.28	LP* Mg	0.17413	s99.99p0.01	22.82
LP O (11)	1.97003	s46.70p53.29	LP* Mg	0.17413	s99.99p0.01	21.86
LP O (14)	1.97015	s46.34p53.66	LP* Mg	0.17413	s99.99p0.01	21.74
LP O (17)	1.96663	s45.22p54.77	LP* Mg	0.17413	s99.99p0.01	23.47

Table 5 shows two strong E(2) that are near to one another. One is from the delocalization of electrons from non-bonding pairs of O (5) and another is from O (2) to the LP Mg having occupancy0.17413e with stabilization energies of 24.71 kcal/mol and 24.64 kcal/mol respectively.In a complex [[Mg(H2O)6](H2O)3]2+, the most powerful engagement is because of the delocalization of the electrons from non-bonding pairs of O (2) to LP Mg with occupancy 0.17514e that balanced this ion by 24.09 kcal/mol. Moreover, the other two nearly equal interactions are seen because of the delocalization of non-bonding pairs of O (8) and O (17) with LP Mg havingstabilization energy of 23.06 kcal/mol and 23.13 kcal/mol respectively. The powerful interactions are presented in Table 6

Table 6. Result of second-order perturbation theory evaluation of Fock matrix within NBO of the complex [[Mg(H2O)6](H2O)3]2+.

Donor NBOs	Occupancy (e)	Hybrid (%)	Acceptor NBOs	Occupancy (e)	Hybrid (%)	$E^{(2)}$ (kcal/mol)
LP O (2)	1.96511	s41.70p58.30d0.00	LP* Mg	0.17514	s99.99p0.01	24.09
LP O (5)	1.96762	s43.30p56.70d0.01	LP* Mg	0.17514	s99.99p0.01	22.55
LP O (8)	1.96754	s44.71p55.29d0.01	LP* Mg	0.17514	s99.99p0.01	23.06
LPO (11)	1.97130	s46.77p53.23d0.01	LP* Mg	0.17514	s99.99p0.01	21.21
LPO (14)	1.96764	s43.23p56.76d0.01	LP* Mg	0.17514	s99.99p0.01	22.57
LP O (17)	1.96763	s45.06p54.94d0.00	LP* Mg	0.17514	s99.99p0.01	23.13

Lastly, in Table 7, the greatest interactions among strong interactions are because of thedelocalization of the electrons from the non-bonding pairs of O (8) with LP* Mg having occupancy of 0.17653e by stabilization energies of 25.21 kcal/mol. The stabilization energies of the remaining three interactions, which are strong, are 23.13 kcal/mol, 22.92 kcal/mol, and 22.16 kcal/mol.

Table 7. Result of second-order perturbation theory evaluation of Fock matrix within NBO of the complex [[Mg(H2O)6](H2O)4]2+.

Donor NBOs	Occupancy (e)	Hybrid (%)	Acceptor NBOs	Occupancy (e)	Hybrid (%)	$E^{(2)}$ (kcal/mol)
LP O (2)	1.96618	$s41.20p58.80d0.00$	LP* Mg	0.17653	$s99.99p0.00d0.01$	23.17
LP O (5)	1.96830	$s43.07p56.93d0.02$	LP* Mg	0.17653	$s99.99p0.00d0.01$	22.16
LP O (8)	1.96308	$s42.10p57.90d0.00$	LP* Mg	0.17653	$s99.99p0.00d0.01$	25.21
LP O (11)	1.97119	$s47.02p52.97d0.01$	LP* Mg	0.17653	$s99.99p0.00d0.01$	21.36
LP O (14)	1.96838	$s43.03p56.97d0.01$	LP* Mg	0.17653	$s99.99p0.00d0.01$	22.06
LP O (17)	1.96827	$s44.77p55.23d0.00$	LP* Mg	0.17653	$s99.99p0.00d0.01$	22.92

4. Conclusions

Natural charge transfer takes place between magnesium ion and the water ligands in complexes [Mg(H2O)6]2+ and [[Mg(H2O)6](H2O)n]2+; n=1-4 has been successfully studied by using NBO Among these five complexes, ligands to ion charge transfer were discovered to be greatest in complex [[Mg(H2O)6](H2O)4]2+ and smallest in complex 2+. The greatest stabilization energy associated with the delocalization of electrons from non-bonding pair of oxygen having LP   Mg was found to be 25.47 kcal/mol in complex [[Mg(H2O)6](H2O)2]2+. The number of stronger interactions was observed to increase with the introduction of ligands within 2nd coordination sphere. The delocalization of electrons from non-bonding pair of oxygen in the initial coordination sphere was greater on which ligand was attached within 2nd coordination sphere than in the other oxygen lone pair.By adding more ligands to the complex's initial coordination sphere, it is possible to intensify the structures, and these intensified structures will lead to drug design.

Conflict of interest

The authors affirm that they have no competing interest.

Author contributions

Conceptualization: Ganesh Prasad Tiwari, Hari Prasad Lamichhane, and Dinesh Kumar Chaudhary. Investigation: Ganesh Prasad Tiwari and Santosh Adhikari. Validation: Hari Prasad Lamichhane and Dinesh Kumar Chaudhary. Article writing (Original draft): Ganesh Prasad Tiwari. Writing-Review: Dinesh Kumar Chaudhary and Hari Prasad Lamichhane. All authors have read and given their consent to the final, printed version of the manuscript.

References

1. Chiu TK, Dickerson RE (2000) 1 Å crystal structures of B-DNA reveal sequence-specific binding and groove-specific bending of DNA by magnesium and calcium. J Mol Biol 301: 915–945. https://doi.org/10.1006/jmbi.2000.4012

2. Serra MJ, Baird JD, Dale T, et al. (2002) Effects of magnesium ions on the stabilization of RNA oligomers of defined structures. *RNA* 8: 307–323. https://doi.org/10.1017/S1355838202024226

3. Misra VK, Draper DE (1998) On the role of magnesium ions in RNA stability. *Biopolymers: OriRes Biomol* 48: 113–135. https://doi.org/10.1002/(SICI)1097-0282(1998)48:2<113::AID-BIP3>3.0.CO;2-Y

4. Lindahl T, Adams A, Fresco JR (1966) Renaturation of transfer ribonucleic acids through site binding of magnesium. *P Natl A Sci* 55: 941–948. https://doi.org/10.1073/pnas.55.4.941

5. Mills BJ, Lindeman RD, Lang CA (1986) Magnesium deficiency inhibits biosynthesis of blood glutathione and tumor growth in the rat. *P Soc Exp Biol Med* 181: 326–332. https://doi.org/10.3181/00379727-181-42260

6. Alfrey AC, Miller NL, Trow R (1974) Effect of age and magnesium depletion on bone magnesium pools in rats. *J Clin Invest* 54: 1074–1081. https://www.jci.org/articles/view/107851

7. Rude RK, Gruber HE (2004) Magnesium deficiency and osteoporosis: animal and human observations. *J Nutr Biochem* 15: 710–716. https://doi.org/10.1016/j.jnutbio.2004.08.001

8. Rude RK, Gruber HE, Norton HJ, et al. (2004) Bone loss induced by dietary magnesium reduction to 10% of the nutrient requirement in rats is associated with increased release of substance P and tumor necrosis factor-α. *J Nutr* 134: 79–85. https://doi.org/10.1093/jn/134.1.79

9. Mohammed HS, Tripathi VD (2020) Medicinal applications of coordination complexes. *J Phys: Conf Ser* 1664: 012070. https://doi.org/10.1088/1742-6596/1664/1/012070

10. Baaij JHD, Hoenderop JG, Bindels RJ (2015) Magnesium in man: implications for health and disease. *Physiol Rev* 95: 1–46. https://journals.physiology.org/doi/full/10.1152/physrev.00012.2014

11. Schwalfenberg GK, Genuis SJ (2017) The importance of magnesium in clinical healthcare. *Scientifica* 2017: 4179326. https://doi.org/10.1155/2017/4179326

12. Sreedhara A, Cowan JA (2002) Structural and catalytic roles for divalent magnesium in nucleic acid biochemistry. *Biometals* 15: 211–223. https://doi.org/10.1023/A:1016070614042

13. Rijal R, Lamichhane HP, Pudasainee K (2022) Molecular structure, homo-lumo analysis and vibrational spectroscopy of the cancer healing pro-drug temozolomide based on dft calculations. *AIMS Biophys* 9: 208–220. https://doi.org/10.3934/biophy.2022018

14. Bock CW, Kaufman A, Glusker JP (1994) Coordination of water to magnesium cations. *Inorg Chem* 33: 419–427. https://doi.org/10.1021/ic00081a007

15. Glendening ED, Feller D (1996) Dication− Water interactions: M2+(H2O)n clusters for alkaline earth metals M= Mg, Ca, Sr, Ba, and Ra. *J Phys Chem* 100: 4790–4797. https://doi.org/10.1021/jp952546r

16. Rodriguez-Cruz SE, Jockusch RA, Williams ER (1999) Hydration energies and structures of alkaline earth metal ions, M2+(H2O)n, n= 5−7, M= Mg, Ca, Sr, and Ba. *J Am Chem Soc* 121: 8898–8906. https://doi.org/10.1021/ja9911871

17. Pavlov M, Siegbahn PE, Sandström M (1998) Hydration of beryllium, magnesium, calcium, andzinc ions using density functional theory. *J Phys Chem A* 102: 219–228. https://doi.org/10.1021/jp972072r

18. Bruzzi E, Raggi G, Parajuli R, et al. (2014) Experimental binding energies for the metal complexes [Mg(NH3)n]2+, [Ca(NH3)n]2+, and [Sr(NH3)n]2+ for n= 4–20 determined from kineticenergy release measurements. *J Phys Chem A* 118: 8525–8532. https://doi.org/10.1021/jp5022642

19. James C, Raj AA, Reghunathan R, et al. (2006) Structural conformation and vibrational spectroscopic studies of 2, 6-bis (p-N, N-dimethyl benzylidene) cyclohexanone using density functional theory. *J Raman Spectrosc* 37: 1381–1392. https://doi.org/10.1002/jrs.1554

20. Frisch MJ, Trucks GW, Schlegel HB, et al. (2016) Gaussian 16 Revision C. 01. 2016; Gaussian Inc.

Wallingford CT. https://gaussian.com/gaussian16/

21. Dennington R, Keith TA, Millam JM (2019) Gaussview version 6. semichem Inc., Shawnee Mission. https://gaussian.com/gaussview6/

22. Becke A (1993) Density-functional thermochemistry.III. The role of exact exchange. J ChemPhys 98: 5648–5652. https://doi. org/10.1063/1.464913

23. Lee C, Yang W, Parr RG (1988) Development of the Colle-Salvetti correlation-energy formula into a functional of the electron density. Phys Rev B 37: 785–789. https://doi.org/10.1103/PhysRevB.37.785

24. Yogeswari B, Tamilselvan KS, Thanikaikarasan S, et al. (2022) Quantum density functional theory studies on additive hydration of tuftsin tetrapeptide. J Nanomaterhttps://doi.org/10.1155/2022/2830708

25. Gangadharan RP, Krishnan SS (2014) Natural bond orbital (NBO) population analysis of 1-azanapthalene-8-ol. Acta Phys Pol A 125: 18–22. http://dx.doi.org/10.12693/APhysPolA.125.18

26. Pokhrel N, Lamichhane HP (2016) Natural bond orbital analysis of [Fe(H2O)6]2+/3+ and [[Zn(H2O)6](H2O)n]2+; n = 0-4. J Phys Chem Biophys 6: 231. http://dx.doi.org/10.4172/2161-0398.1000231.

2022-end editorial: achievements, thanks, perspectives

Carlo Bianca1,* and Lombardo Domenico2,*

1 Efrei Research Lab, Paris-Panthéon-Assas University, France
2 Consiglio Nazionale delle Ricerche, Istituto per i Processi Chimico-Fisici, 98158 Messina, Italy

1. Journal summary from co-Editor in Chief

Now we have stepped into 2023, at the beginning of the new year, and together with the Editorial Office of AIMS Biophysics, we wish to testify my sincere gratitude to all authors, members of the editorial board, and reviewers, thanking everyone for their contribution to AIMS Biophysics in 2022, now we hope we could cooperate with you more this year. AIMS Biophysics is an international Open Access journal founded in 2014 and devoted to publishing peer reviewed, high-quality, original papers in the field of biophysics. The statistics and metrics of the journal have been increased and remarkable are the following achievements:-About 30 publications in 2022 (3 review papers, 23 research articles, 4 editorials);- A total of four special issues were issued in 2022, and it is hoped that these four special issues will attract more contributions from authors in 2023. 4 special issues have reached more than 5 papers.

In particular, the new topics of the special issues proposed in 2022 have allowed the interplay between different scholars coming from different research fields. AIMS Biophysics invited nine experts to join our editorial board in 2022. In the next year 2023, we hope that we can increase the quantity and quality of papers submitted to AIMS Biophysics and constantly seek scholars with good backgrounds to join the editorial board. Shorten the article processing cycle and improve efficiency. Strive to establish a special issue with topical and hot topics, attract more relevant manuscripts, increase citations/papers and total citations, and improve the academic ranking of AIMS Biophysics.

Finally, we would like to thank all the editorial board members again. The development and progress of the magazine can not be separated from your strong support and time. In the coming year of 2023, we look forward to further strengthening the magazine's strength through continued cooperation.

Prof. Carlo Bianca co-Editor in Chief
Prof. Lombardo Domenico co-Editor in Chief
AIMS Biophysics

2. Editorial development

2.1. Manuscripts statistics

Manuscript statistics (2022)
Reject rate: 45.3%
Publication time (median time from submission to online): 76 days

2.2. Author distribution
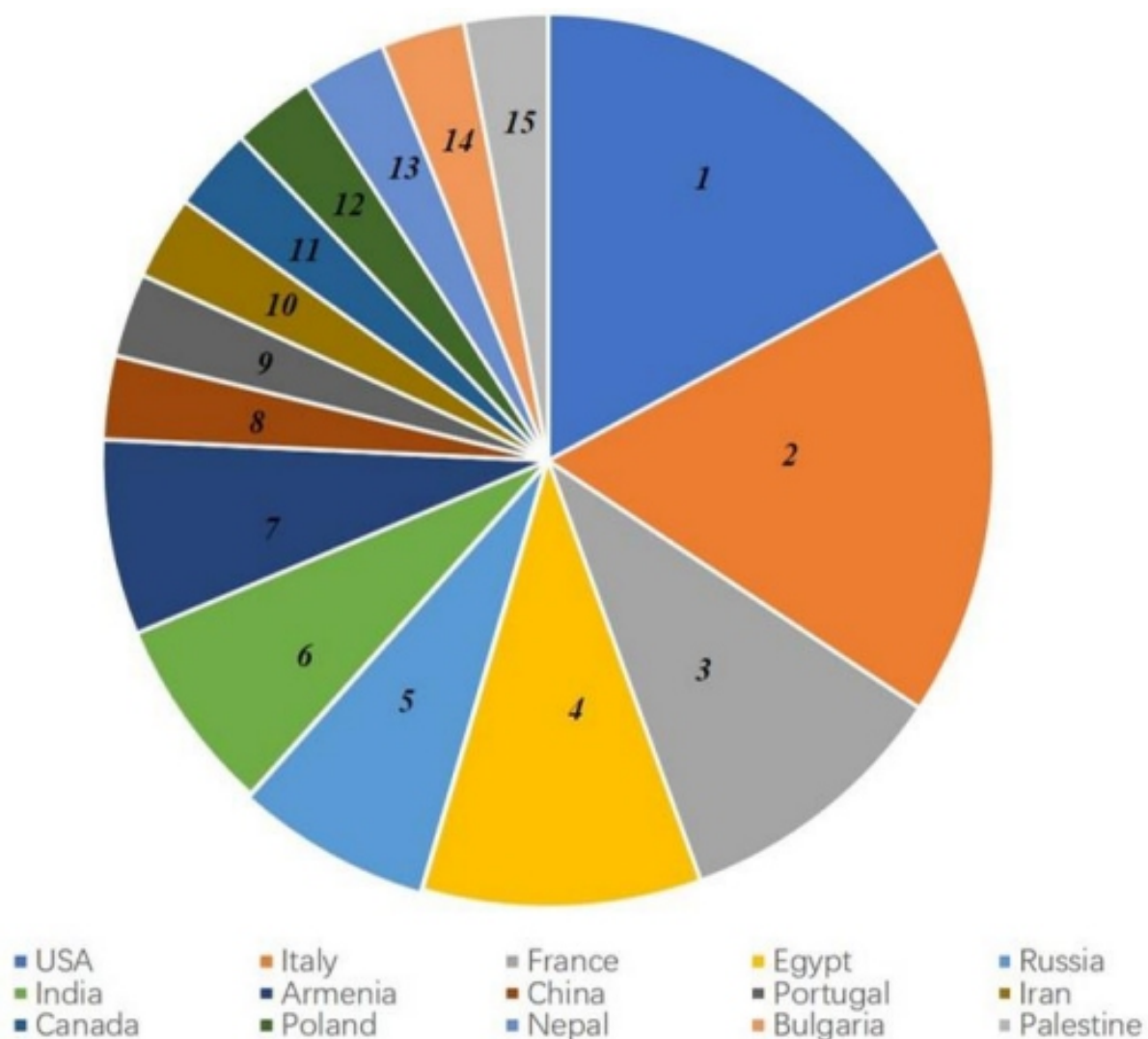
2.3. Articles type

Type	Number
Review	3
Research article	23
Editorial	4

2.4. Articles metrics
The top 10 articles with the highest citations for the past five years:

Title	Citations
Recent progress in Monte Carlo simulation on gold nanoparticle radiosensitization	21
Charged amino acids may promote coronavirus SARS-CoV-2 fusion with the host cell	16

Title	Viewed
Intrinsic blue-green fluorescence in amyloyd fibrils	13
Interdisciplinary approaches to the study of biological membranes	12
Functional characterizations of polyethylene terephthalate-degrading cutinase-like enzyme Cut190 mutants using bis(2-hydroxyethyl) terephthalate as the model substrate	10
Macromolecular sizes of serum albumins in its aqueous solutions	8
Biochemical and biophysical mechanisms underlying the heart and the brain dialog	6
Nanoparticle-based delivery platforms for mRNA vaccine development	6
Thermodynamic, kinetic and docking studies of some unsaturated fatty acids-quercetin derivatives as inhibitors of mushroom tyrosinase	6
A machine learning algorithm for identifying and tracking bacteria in three dimensions using Digital Holographic Microscopy	6

The top 10 articles with the highest viewed for the past two years:

Title	Viewed
Toxicity associated with gadolinium-based contrast-enhanced examinations	5184
An efficient method of detection of COVID-19 using Mask R-CNN on chest X-Ray images	3621
Effects of magnetic field treated water on some growth parameters of corn (Zea mays) plants	3076
A basic introduction to single particles cryo-electron microscopy	1874
Screening coronavirus and human proteins for sialic acid binding sites using a docking approach	1831
Sequence–function correlation of the transmembrane domains in NS4B of HCV using a computational approach	1724
Radioprotective effect of nanoceria and magnetic flower-like iron oxide microparticles on gamma radiation-induced damage in BSA protein	1701
Chest X-Ray image and pathological data based artificial intelligence enabled dual diagnostic method for multi-stage classification of COVID-19 patients	1631
Tumor treating fields (TTFs) using uninsulated electrodes induce cell death in human non-small cell lung carcinoma (NSCLC) cells	1452
Evaluation of dose enhancement with gold nanoparticles in kilovoltage radiotherapy using the new EGS geometry library in Monte Carlo simulation	1396

2.5. Special issue
2.5.1. New special issues
1. Importance of modelling and simulation in biophysical applications;
2. Electromagnetic waves and biology;
3. Scientific advances in complex systems of biophysical interest;
4. Scientific Advance in Biomembranes and Biomimetic Membranes of Biophysical Interest

2.5.2. Special issues with more than 5 papers
Scientific advances in complex systems of biophysical interest
https://www.aimspress.com/aimsbpoa/article/6201/special-articles
Interplay and Multiscale Modeling of Biological Complex Systems
https://www.aimspress.com/aimsbpoa/article/6057/special-articles
Methodological trends in structural biology 2021
https://www.aimspress.com/aimsbpoa/article/5840/special-articles
Applications of artificial intelligence, mathematical modeling and simulation in medical biophysics
https://www.aimspress.com/aimsbpoa/article/5637/special-articles

2.6. Editorial board members
AIMS Biophysics has a total of 43 editors, 9 of whom were newly invited in 2022.
2.7. Summary and plan
2.7.1. Summary
In the past year, we published 30 articles, created 4 special issues, and invited 9 new editorial board members. The development of articles and special issues is stable and all aspects go hand in hand.

2.7.2. Plan in 2023
Strive to speed up the process of journal processing, hoping that the median processing time from receiving to publishing online next year is stable and less than 50 days; At the same time, both the appointment and processing of manuscripts should be in strict accordance with the standards, hoping to attract high manuscript quality through the level accumulation of journals. Only by laying a good foundation of the most fundamental quality will the possibility of journals being included in various excellent databases increase, thus improving the popularity of journals. Our ultimate goal seeks to be indexed by more databases by 2023.

Identification of potential SARS-CoV-2 papain-like protease inhibitors with the ability to interact with the catalytic triad

Murtala Muhammad1,2,*, I. Y. Habib3, Abdulmumin Yunusa1, Tasiu A. Mikail1, A. J. Alhassan4, Ahed J. Alkhatib5, Hamza Sule6, Sagir Y. Ismail1 and Dong Liu2,*

1 Department of Biochemistry, Kano University of Science and Technology, Wudil, Nigeria
2 College of Life Science, Hebei Normal University, 050024 Shijiazhuang, China
3 Department of Chemistry, Sa'adatu Rimi College of Education Kumbotso, Kano, Nigeria
4 Department of Biochemistry, Bayero University Kano, Nigeria
5 Faculty of Medicine, Jordan University of Science and Technology, Jordan
6 Department of Applied Medical Science, Bayero University, Kano, Nigeria

ABSTRACT

Severe acute respiratory syndrome corona virus2 (SARS-CoV-2) is responsible for the current pandemic that led to so many deaths across the globe and still has no effective medication. One attractive target is Papain-like protease (Plpro), which plays a critical role in viral replication.Several important structural features dictate access to the PLpro narrow active site, which includes a series of loops surrounding the area. As such, it is difficult for chemical compounds to fit the SARS-CoV-2 PLpro active site. This work employed a computational study to discover inhibitorsthat could bind to the SARS-COV-2 PLpro active site, mainly by virtual screening, molecular dynamic simulation, MMPBSA and ADMET analysis. Eight potential inhibitors were identified:carbonoperoxoic acid, Chrysophanol-9-anthrone, Adrenolutin, 1-Dehydroprogesterone, Cholest-22-ene-21-ol, Cis-13-Octadecenoic acid, Hydroxycarbonate and 1-(4-(4-Methylphenyl)-5-phenyl-1,3-oxazol-2-yl) isoquinoline, with binding scores of −4.4, −6.7, −5.9, −6.7, −7.0, −4.6, −4.5 and −5.6 kcal/mol, respectively. All these compounds interacted with critical PLpro catalytic residues and showed stable conformation in molecular dynamics simulations with significant binding energies of −12.73 kcal/mol, −10.89 kcal/mol, −7.20 kcal/mol, −16.25kcal/mol, −19.00 kcal/mol, −5.00 kcal/mol, −13.21 kcal/mol and −12.45 kcal/mol, respectively, as revealed by MMPBSA analysis. ADMET analysis also indicated that they are safe for drug development. In this study, we identified novel compounds that interacted with the key catalytic residues of SARS-CoV-2 PLpro with the potential to be utilized for anti-Covid-19 drug development.

Keywords: SARS-CoV-2; PLpro; inhibitors; molecular docking; molecular dynamics simulations; MMPBSA

1. Introduction

Emerging and re-emerging infectious diseases remain among the greatest threats to human survival on this planet. Animal Pathogens mutate and evolve continuously, gaining the ability to become zoonotic or less susceptible to treatment [1].

Coronaviruses are enveloped RNA viruses distributed broadly among reptiles, mammals and birds, causing respiratory, enteric, hepatic and neurologic diseases. Recently, a severe human respiratory illness believed to be of animal origin has been responsible for several deaths across the globe [2–4].

The disease has been declared a global health emergency by the World Health Organization (WHO) [4]. Studies suggested that a new highly infectious strain of Coronavirus (SARS-CoV-2) is responsible for the pandemic [3]. So far, there is no globally accepted standard therapeutic for its management [2].Papain-like protease (PLpro) is a coronavirus enzyme that plays an essential role in viral replication and pathogenesis. It converts viral polyprotein into a functional replicase complex [5]. PLpro exhibits deubiquitinating and deISG15ylating (interferon-induced gene 15) activities in SARS-CoV and MERS-CoVs [6–9]. The catalytic triad Cys111, His272 and Asp286 is located at the interface between the thumb and palm sub-domains of the enzyme [6,10,11]. Small chemical compounds and natural products are rich sources of lead compounds that could be explored for new drug development. With the recent advancement in computational chemistry, chemical libraries could be screened for compounds that could interact with biological structures and inhibit the proliferation and survival of pathogens [12–14]. Several scientists have screened various chemical libraries in an attempt to discover potent PLpro inhibitors. For instance, Alamri etal. identified three compounds from a library of more than six thousand protease inhibitors, Hajbabaie etal. screened more than thirty thousand compounds, Peng etal. identified four promising PLpro inhibitors from a 1.6 million compound library, and many other similar studies were reported with varying success stories [15,16].

Computational ligand-target prediction has proven reliable in drug discovery [7]. Recent in-vitro studies imply that Plpro inhibitors that bind to the active or ubiquitin-binding sites are promising candidates for drug development [6]. C. occidentalis was reported to have demonstrated remarkable ethnomedicinal properties such as antimicrobial activity, anti-viral properties, anti-carcinogenicity, anti-proliferation properties and antioxidant properties [17]. Therefore, the present study will utilize in silico techniques to identify potent Covid-19 PLpro inhibitors with the ability to interact with the PLpro catalytic residues from C. occidentalis phytochemicals National Cancer Institute (NCI) and PubChem chemical compounds databases for anti-COVID-19 drug development.

2. Materials and methods

2.1. Ligand retrieval and preparation

More than Fifty C. occidentalis phytochemicals were obtained from the literature [18,19], as well as Six thousand chemical compounds from the NCI library (https://dtp.cancer.gov/) and PubChem (https://pubchem.ncbi.nlm.nih.gov/) databases, for the virtual screening. The NCI compounds employed in this study are NCI diversity set VI compounds tested in the NCI human tumor cell line screening, while the PubChem compounds were obtained from the PubChem similarity search of C. occidentalis phytochemicals that bind to the PLpro active site. The Ligands in SDF format were minimized and converted to PDBQT with PyRx-OpenBabel software.

2.2. Protein target preparation

The PDB structure of SARS-CoV-2 PLpro was retrieved from the Protein Data Bank (https://www.rcsb.org) (PDB ID: 7cmd). All hetero atoms were removed from the protein molecule using Discovery Studio software.

2.3. Molecular docking and docking validation

Molecular docking validation was conducted by re-docking the native ligand (GRL0617) of the 7cmd crystal structure to PLpro. Accordingly, GRL0617 was separated from the protein and prepared for docking using Discovery Studio (Version 20). The ligand was then docked back into PLpro's active site using Auto Dock Vina. The docked complex was superimposed with the X-ray resolved crystal Plpro (7cmd) bearing the co-crystallized ligand, and the root mean square deviation (RMSD) value was

generated in PyMOL [20]. Site-directed docking around the PLpro active site was performed with all the Ligands. The receptor molecule remains rigid, and the ligands are flexible. Binding interactions were analyzed using Discovery Studio [21]. Only compounds that interacted with the PLpro key catalytic residues will be considered for further studies.

2.4. Molecular dynamics simulation

Molecular dynamics (MD) simulations of the protein and protein-ligand complexes were performed with a GROMACS 5.0 package [22], using Amber99SB force field and TIP3P water mode, under periodic boundary conditions with a dodecahedron periodic box set at a minimum distance of 1.0 between the protein and edge of the box. The system was neutralized with 0.154 moles/liter NaCl. The initial energy minimization process was conducted by applying a simulated annealing method with a corresponding equilibration of 1ns NVT and 1ns NPT. MD simulation production was performed at a constant temperature and pressure of 300 K and 1 atm, respectively, with a time step of 2 fs. The simulation was run in triplicate for 100 ns. Root mean square deviation (RMSD) and root mean square fluctuation (RMSF) were calculated to determine the stability of the protein-ligand complex [23].

2.5. Binding free-energy calculations using MMPBSA

The protein-ligand complexes' binding free energies (ΔG_{bind}) were computed using the Molecular Mechanics Poisson-Boltzmann Surface Area (MM-PBSA) algorithm, which gives a more accurate estimation of the free binding energy than the scoring function of docking experiments [24]. The GROMACS compatible g_mmpbsa tool package was used to implement the MM-PBSA calculations, and the Python script MmPbSaStat.py provided in the g_mmpbsa package compiled and estimated the interaction free energies [25]. The total binding free energy (ΔG_{total}) is determined as the total energy released from the ligand-protein complex, which is contributed by molecular mechanics binding energy (ΔE_{MM}) and solvation free energy (ΔG_{sol}) using the following equations:

$$\Delta E_{MM} = \Delta E_{int} + \Delta E_{ele} + \Delta E_{vdw}$$

$$\Delta G_{sol} = \Delta G_{pl} + \Delta G_{np}$$

$$\Delta G_{total} = \Delta E_{MM} + \Delta G_{sol}$$

$$AG_{bind} \text{ (MM-PBSA)} = \Delta E_{MM} + \Delta G_{sol} - \Delta T \Delta S$$

where ΔE_{int} stands for internal energy, ΔE_{ele} represents electrostatic energy, ΔE_{vdw} is for vander Waals energy, ΔG_{pl} is for polar energy, ΔG_{np} is for non-polar energy components, and ΔG_{sol} is the contribution to total solvation free energy, while ΔG_{bind} stands for the free energy of binding evaluated after entropic calculations $-\Delta T \Delta S$ [26].

2.6. ADMET analysis

SwissADME (www.swissadme.ch) and ADMETSAR (http://lmmd.ecust.edu.cn/admetsar2/) servers were employed to evaluate the metabolic and toxicological properties of the Ligands. The canonical format of the chemical compounds was used as the entry system for ADMET (absorption, distribution, metabolism and toxicity) calculations [27].

3. Results
3.1. Molecular docking
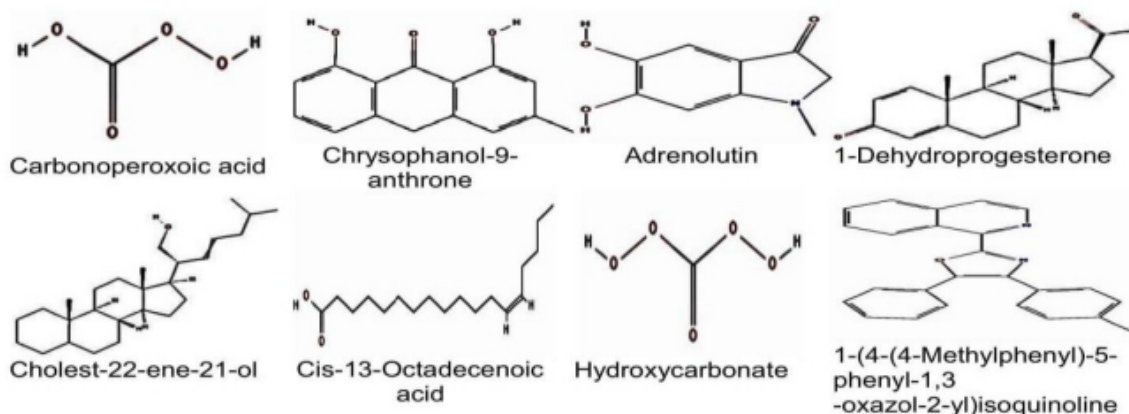
Figure1. Chemical structures of the identified ligands.

Table1. Binding scores and PLpro residues' interactions with the Ligands.

| Compound Name	PubChem CID	Binding Score (kcal/mol)	Hydrogen Bond Interaction	Other Interactions
Carbonoperoxoic acid	181880	−4.4	**Asp 286**, Ile 285, Tyr 273	Leu 118, Thr 115, His 275, Ala 114, Trp 106, Lys 274, **Cys 111** and Gly 287
Chrysophanol-9-anthrone	68111	−6.7	Ser 212, Tyr 305, Glu 214	Glu 252, Tyr 251, Tyr 213, Thr 257 and Lys 254
Adrenolutin	12556	−5.9	His 175, Ala 153, Arg 82, Asn 156	His 73, Phe 79, Thr 74, Cys 155, Tyr 154 and Asp 76
1-Dehydroprogesterone	247929	−6.7	Lys 232	Leu 185, Thr 207, Met 208, Arg 166, Leu 199, Glu 203, Val 202, Ser 170 and Met 206
Cholest-22-ene-21-ol	129883894	−7.0	Ser 278	Thr 277, Lys 279, Gln 122, Gly 256, Thr 257, Tyr 305, Lys 217, Tyr 213, Lys 306, Thr 259

				and Phe 258
Cis-13-Octadecenoic acid	5312441	−4.6	Asn 110, **Cys 111**	Gly 287, **Asp 286**, Asp 108, **His 272**, Asn 109, Ala 107, Ala 288, Lys 105, Trp 106, and Leu 289
Hydroxycarbonate	17887040	-4.5	His 275, Ile 285 and Ser 103	**Cys 111, Asp 286**, Tyr 273, Lys 274, Ala 114, Trp 106 and Thr 115
1-(4-(4-Methylphenyl) -5-phenyl-1,3 -oxazol-2-yl)isoquinoline	272358	−5.6	Trp 106	**Asp 286, His 272**, Lys 274, Lys 105, Thr 265 and Ala 288

Structural-based virtual screening was employed to find the potential inhibitors of SARS-CoV-2 PLpro. The docking and scoring functions were validated before the docking was carried out. Compounds that interacted with the catalytic site residues of PLpro were selected for further studies (Figure 1). Carbonoperoxoic acid and hydroxycarbonate were identified from the PubChem similarity search of the C. occidentalis phytochemicals that bind to the active site, while 1-(4-(4-Methylphenyl)-5-phenyl-1,3-oxazol-2-yl)isoquinoline was identified from the NCI diversity set VI library, and the remaining five compounds are Cassia spp. phytochemicals. The selected chemical compounds have binding scores ranging from −4.4 to 7.0 kcal/mol. Carbonoperoxoic acid, Chrysophanol-9-anthrone, Adrenolutin, 1-Dehydroprogesterone, Cholest-22-ene-21-ol, Cis-13-Octadecenoic acid,Hydroxycarbonateand1-(4-(4-Methylphenyl)-5-phenyl-1,3-oxazol-2-yl)isoquinoline showed binding scores of−4.4,−6.7,−5.9,−6.7,−7.0,−4.6,−4.5 and−5.6 kcal/mol, respectively (Table 1).

3.2. Analysis of the ligands' interactions
The 2D interactions of the eight selected ligands and the SARS CoV-2 PLpro complexes were visualized with the Discovery Studio software. As shown in Table 1 and Figure 2, carbonoperoxoicacid binds within the active site of SARS CoV-2 PLpro, forming hydrogen bonds with Asp 286, Ile 285 and Tyr 273 residues. It also formed hydrophobic interaction with Cys 111 and other active site residues, such as Leu 118, Thr 115, His 275, Ala 114, Trp 106, Lys 274 and Gly 287 (Figure 2a).Chrysophanol-9-anthrone formed three hydrogen bonds with Ser 212, Tyr 305 and Glu 214 and hydrophobic bonds with Glu 252, Tyr 251, Tyr 213, Thr 257 and Lys 254 (Figure 2b).Adrenolutin also interacted with His 175, Ala 153, Arg 82, Asn 156 through hydrogen bonds, with six other, hydrophobic bonds: His 73, Phe 79, Thr 74, Cys 155, Tyr 154 and Asp 76 (Figure 2c).1-Dehydroprogesterone formed only one hydrogen bond with Lys 232 and many other hydrophobic interactions with the nearby active site residues, such as Leu 185, Thr 207, Met 208, Arg 166, Leu 199, Glu 203, Val 202, Ser 170 and Met 206 (Figure 2d).Cholest-22-ene-21-ol also forms only one hydrogen bond with Ser 278. It also interacts through hydrophobic bonding with Thr 277, Lys 279, Gln 122, Gly 256, Thr 257, Tyr 305, Lys 217, Tyr 213, Lys 306, Thr 259 and Phe 258 (Figure 2e).Cis-13-Octadecenoic acid interacted with all the catalytic triads of SARS-CoV-2 PLpro. It forms a hydrogen bond with Cys 111 and hydrophobic interaction with Asp 286 and His 272. Others include an additional hydrogen bond with Asn 110 and hydrophobic interactions with Gly 287, Asp 108, Asn 109, Ala 107, Ala 288, Lys 105, Trp 106 and Leu 289 (Figure

2f). Because the structure of cis-13-Octadecenoic acid is long, a large part of the molecule is placed outside the active site and lies under the blocking loop 2 (BL2) in the palm sub-domain. Hydroxycarbonate forms three hydrogen bonds with His 275, Ser 103 and Ile 285 and vander Waals interactions with catalytic Cys111 and Asp 286.Other important interactions include Tyr 273, Lys 274, Trp 104 and Ala 114 (Figure 2g). On the other hand,1-(4-(4-Methylphenyl)-5-phenyl-1,3-oxazol-2-yl) isoquinoline forms a Pi-cation bond with Asp 286, Pi-anion bond with Lys 274 and Pi-donor hydrogen bond with Trp 106. Other significant interactions are His 272, Thr 265, Lys 105, Leu 289 and Ala 288 (Figure 2h).
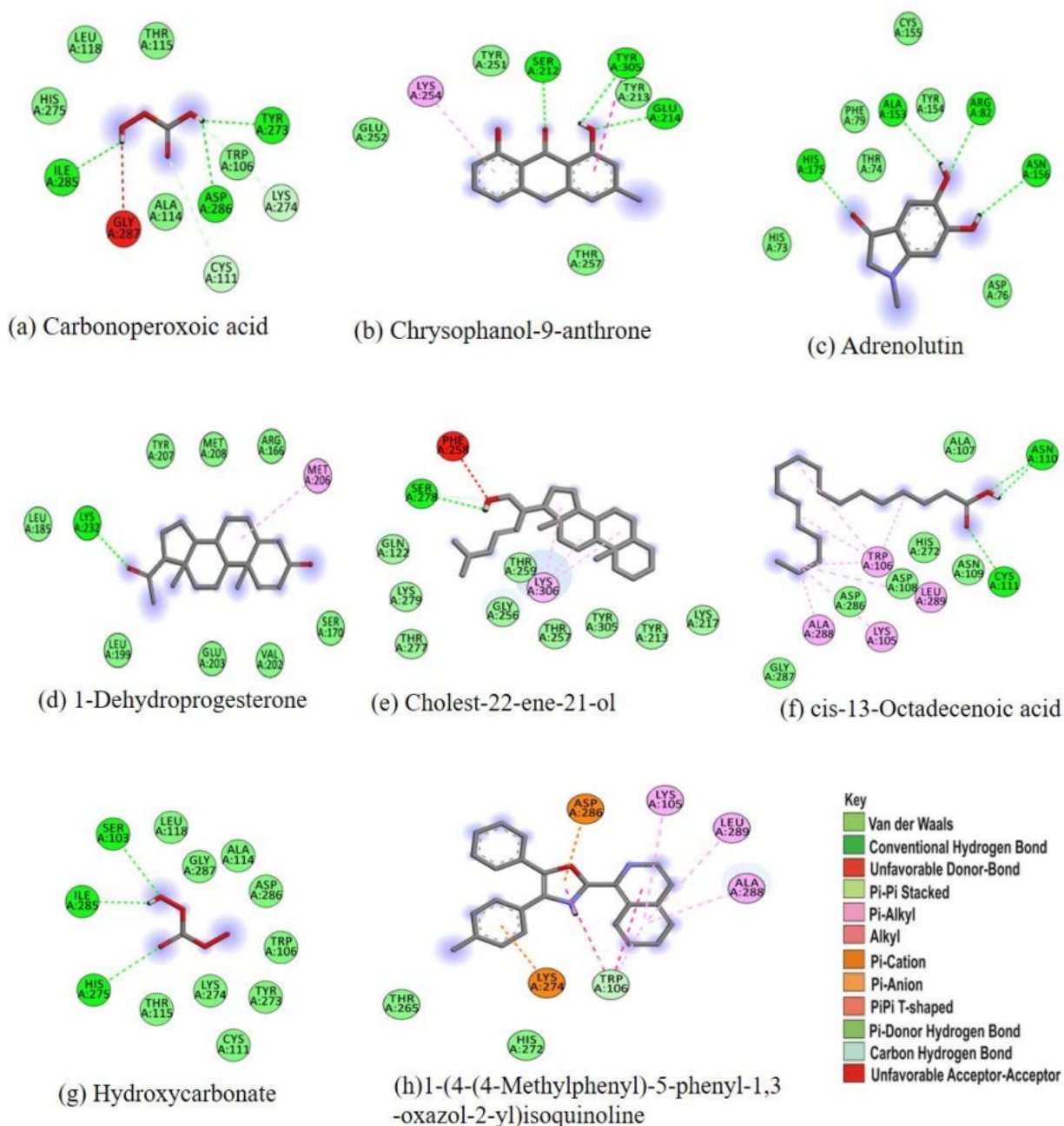

Figure 2. 2 D depiction of SARS-CoV-2 PLpro-Ligands' interactions complexes.

3.3. Molecular dynamics (MD) simulation

MD simulation is a widely used computational method for analyzing the ligand-protein complex dynamic behavior and stability under different conditions [23]. The simulation results were analyzed by RMSD and RMSF.

3.3.1. Root mean square deviation (RMSD)

The structural changes in protein-ligand complex and dynamic behavior were analyzed by the

RMSD and are presented in Figure 3.
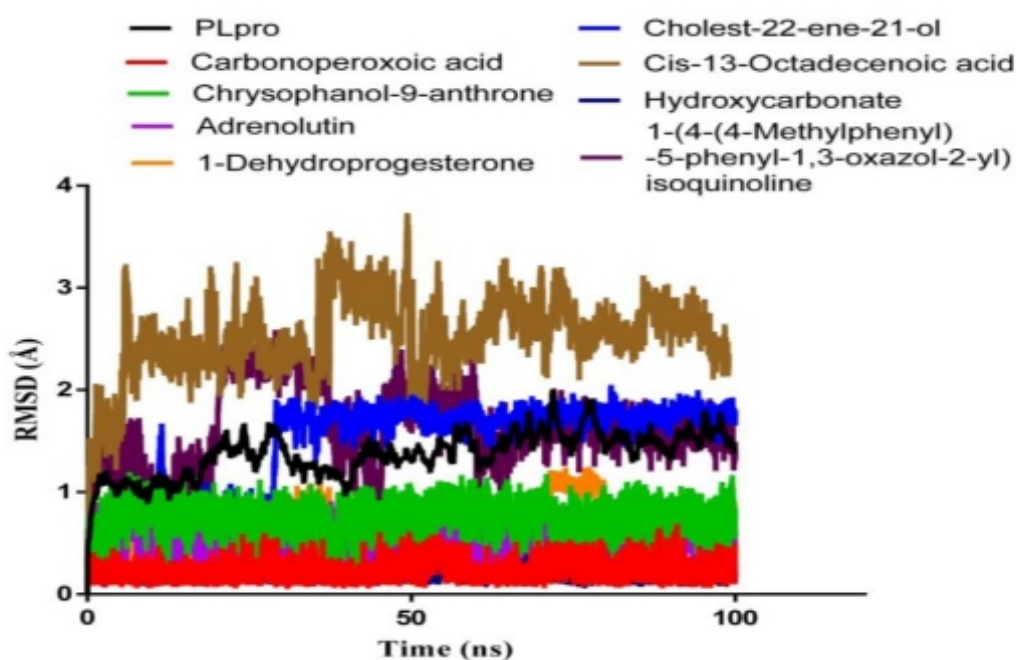
Figure 3. Plots of RMSD of the PLpro-ligands complex.

The results show that Carbonoperoxoic acid is highly stable at the active site of PLpro with a single binding mode; it fluctuates around 0.1 and 0.6 Å, with an average RMSD of 0.22 Å, which is even more stable than the Apo-protein. While Chrysophanol-9-anthrone reached stability at around 10 ns, it fluctuated between 0.2 and 1.2 Å, with an average RMSD of 0.75 Å. Adrenolutin is highly stable; it fluctuates around 0.6 Å throughout the simulation and has an average RMSD value of 0.62Å.1-Dehydroprogesterone has two major fluctuations around 40 ns and 70 ns but becomes stable after 80 ns of the simulation. Similarly, Cholest-22-ene-21-ol becomes stable at around 30 ns following a large fluctuation at the beginning of the simulation, with an average RMSD of 1.43 Å.Cis-13-Octadecenoic acid remains stable but at a higher average RMSD that ranges between 2.06 and 3.55 Å and has a large fluctuation between 30 and 50 ns of the simulation. Hydroxycarbonate is also stable at the PLpro active site; it fluctuates between RMSD of 0.09 and 0.5 Å throughout the simulation, with an average RMSD value of 0.25 Å. 1-(4-(4-Methylphenyl)-5-phenyl-1,3-oxazol-2-yl)isoquinoline has two significant fluctuations between 16ns and 40ns and between 45 ns and 60 ns but stabilized from 60 ns till the end of the simulation.

3.3.2. Root mean square fluctuation (RMSF)

RMSF analysis was conducted to explore the per-residue fluctuations of the system. RMSF analysis showed that binding of the ligands does not affect the stability of the PLpro catalytic triad residues, Cys 111, Asp 286 and His 272 (Figure 4). The RMSF value of the Apo-protein reached equilibrium after an initial increase within the first 1ns, with an average RMSF of 1.2 Å.
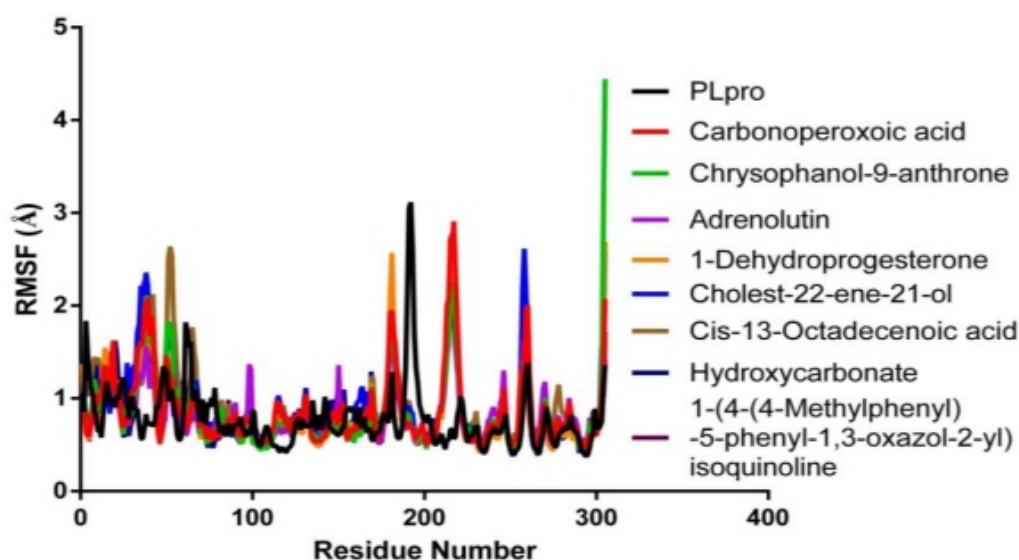
Figure 4. The root mean square fluctuation (RMSF).

As shown in Figure 4, the Apo-protein fluctuations during the simulation are shown in black color; its major fluctuations are at the residues from 66 to 75 (1.82 Å), 193 to 209 (2.1 Å) and 265 to 271 (1.41 Å). Carbonoperoxoic acid-PLPro complex, shown in red, has major fluctuations between residues 40 and 55 (2.03 Å), 183 and 196 (1.93 Å) and 264 and 271 (1.36 Å). Similarly, chrysophanol-9-anthrone-PLPro complex, shown in green, has fluctuations between 42 and 53 (2.09 Å), 189 and 193 (1.78 Å) and 219 and 230 (2.21 Å), similar to those of carbonoperoxoic acid.Adrenolutin-PLPro complex (purple) had major fluctuations between residues 43 and 50 (1.56 Å),189 and 196 (1.77 Å) and 214 and 230 (2.21 Å). 1-dehydroprogesterone-PLPro complex (orange) causes fluctuations around residues 14 to 33 (1.55 Å), 41 to 55 (1.93 Å), 188 to 195 (2.57 Å) and 221 to 230 (2.75 Å). In contrast, Cholest-22-ene-21-ol-PLPro complex (represented in blue color) fluctuates at residues between 39 and 55 (2.36 Å), 189 and 192 (1.97 Å), 215 and 230 (2.46 Å) and 260 and 271 (2.62 Å), with an average RMSF higher than that of the Apo-protein.Cis-3-octadecenoic acid-PLPro complex (brown) major fluctuations are at the residues between 43 and 56 (2.13 Å), 59 and 67 (2.64 Å), 188 and 195 (1.86 Å) and 219 and 230 (2.69 Å). Hydroxycarbonate- PLPro complex (represented in navy blue) major fluctuations are between residues 36 and 55 (1.65 Å), 188 and 194 (1.67 Å), 222 and 230 (2.76 Å) and 264 and 271 (2.09Å).1-(4-(4-Methylphenyl)-5-phenyl-1,3-oxazol-2-yl)isoquinoline-PLPro complex fluctuates around residues 42 to 53 (2.26 Å), 189 to 193 (2.01 Å) and 218 to 235 (2.11 Å).

3.4. Binding free energy of the PLpro-ligands complex using MMPBSA

The binding free energy was calculated to understand more about the interactions between PLpro and the ligands.

Table 2. Binding free energy of the PLpro in complex with the ligands.

Ligand-PLpro Complex	Vander Waals Energy (kcal/mol)	Electrostatic Energy (kcal/mol)	Polar Solvation Energy (kcal/mol)	Apolar Energy (kcal/mol)	Total Binding Energy (kcal/mol)
Carbonoperoxoic acid	−10.70 ±1.81	−20.46 ± 2.50	20.60 ± 1.39	−2.17 ± 0.02	−12.73 ± 1.39
Chrysophanol-9-anthrone	−22.12 ± 1.41	−2.90 ± 1.66	16.49 ± 2.49	−2.36 ± 0.08	−10.89 ± 2.05
Adrenolutin	−12.73 ± 1.98	−13.59 ± 2.37	21.31 ± 1.39	−2.18 ± 0.14	−7.20 ± 1.48
1−dehydroprogesterone	−21.61 ± 1.92	−4.43 ± 1.66	12.26 ± 2.07	−2.47 ± 0.10	−16.25 ± 1.72
Cholest-22-ene-21-ol	−22.57 ± 2.00	−12.51 ± 2.09	19.15 ± 1.38	−2.90 ± 0.12	−19.00 ± 1.83
Cis-13-Octadecenoic acid	−7.76 ± 0.66	−28.89 ± 2.63	32.96 ± 2.81	−1.22 ± 0.09	−5.00 ± 0.92
Hydroxycarbonate	−12.75 ± 2.26	−24.00 ± 3.32	26.12 ± 2.23	−2.57 ± 0.06	−13.21 ± 1.61
1-(4-(4-Methylphenyl)-5-phenyl-1,3-oxazol-2-yl)isoquinoline	−17.62 ± 1.43	−2.62 ± 0.86	10.31 ± 1.67	−2.52 ± 0.11	−12.45 ± 1.77

As shown in Table 2, the binding energies of the eight complexes range from −19.00 kcal/mol to −5.00 kcal/mol. Overall, Cholest-22-ene-21-ol shows the highest binding energy, followed by 1-Dehydroprogesterone. In contrast, Cis-13-Octadecenoic acid has the least binding energy.

3.5. MMPBSA energy decomposition analysis of the residue-ligand interactions
Binding free energy decomposition analysis was conducted to gain insight into the residues' contributions to the whole system. The energy contribution for each residue is shown in Figure 5.
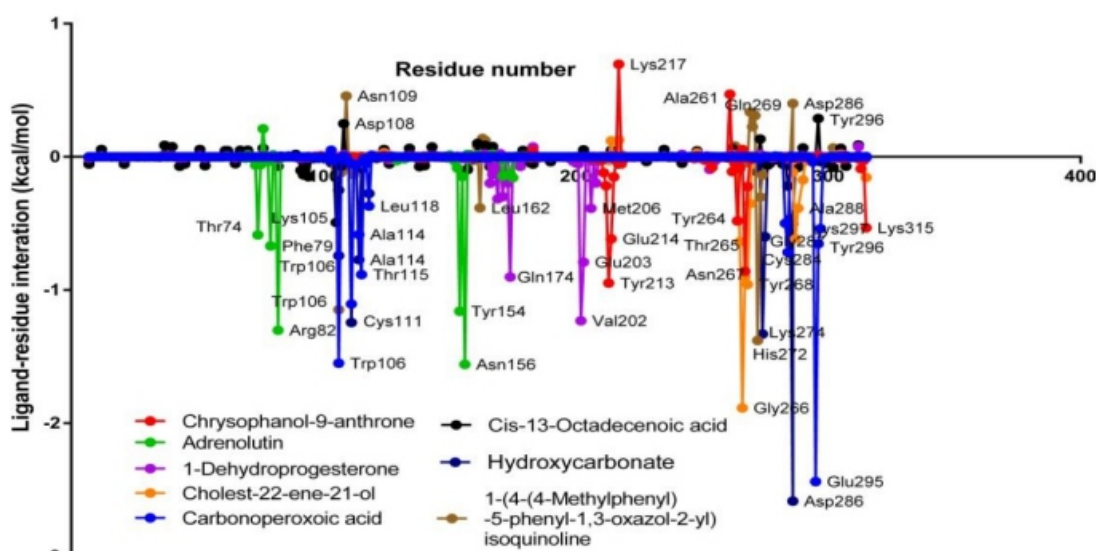
Figure 5. Energy spectra of the PLpro residues' interaction with the Ligands.

Notably, the energy contributions of the carbonoperoxoic acid-PLpro complex residues include catalytic Cys111(−1.104 kcal/mol), Tyr106(−1.549 kcal/mol), Thr115(−0.88 kcal/mol), Ala114(−0.58kcal/mol), Leu118(−0.37 kcal/mol), Cys284(−0.72 kcal/mol), Tyr283(−0.49 kcal/mol), Glu295(−2.44kcal/mol), Tyr296(−0.65 kcal/mol) and Lys297(−0.54 kcal/mol). Similarly, the major binding energy contributing residues in Chrysophanol-9-anthrone-PLpro complex are Tyr213(−0.95 kcal/mol),Glu214(−0.62 kcal/mol), Asn267(−0.86 kcal/mol), Tyr264(−0.48 kcal/mol), Tyr268(−0.22 kcal/mol) and Lys315(−0.53 kcal/mol). On the other hand, Lys217 and Ala261 binding energies wereunfavorable. Adrenolutin–Plpro complex binding energy was contributed by Thr74 (−0.59 kcal/mol),Phe79 (−0.67 kcal/mol), Arg82 (−1.30 kcal/mol), Tyr154 (−1.16 kcal/mol) and Asn156 (−1.56kcal/mol). Meanwhile, for1-dehydroprogesterone-PLpro complex, they are Gln174(−0.901 kcal/mol),Val202(−1.23 kcal/mol), Glu203(−0.79 kcal/mol) and Met206(−0.39 kcal/mol). Furthermore,Cholest-22-ene-21-ol-PLpro complex residues with obvious binding energy contributions are Gly266(−1.89 kcal/mol), Tyr268(−0.96 kcal/mol), Asn267(−0.90 kcal/mol), Thr265(−0.64 kcal/mol),Gln269(−0.35 kcal/mol), Gly288(−0.62 kcal/mol), Ala288(−0.39 kcal/mol) and Leu290(0.17kcal/mol). Hydroxycarbonate-PLpro complex residues with enormous energy contributions are Try106(−0.74 kcal/mol), Cys111(−1.24 kcal/mol), Ala114(−0.77 kcal/mol), Leu118(−0.28 kcal/mol), Lys274(−1.33 kcal/mol), Asp286(−2.58 kcal/mol), Ile285(−0.46 kcal/mol), His272(0.11 kcal/mol), Asp286 (−0.50 kcal/mol) and His275(−0.6 kcal/mol). Finally,1-(4-(4-Methylphenyl)-5-phenyl-1,3-oxazol-2-yl)isoquinoline–Plpro complex binding energy contributing residues include Leu162(−1.38 kcal/mol) and Trp106(−0.30 kcal/mol), while Gln269,Asn109 and Asp286 have unfavorable binding energy.

3.6. Drug-likeness properties and ADMET screening

Table 3. Properties of the identified compounds.

Name	Log p	Log s	Rotatable bonds	Hydrogen bond acceptors	Hydrogen bond donors
Carbonoperoxoic acid	0.154	−0.07	1	4	2
Chrysophanol-9-anthrone	2.54142	−4.07	0	3	2
Adrenolutin	0.7303	−1.87	0	3	2
1-Dehydroprogesterone	4.4995	−4.28	1	2	0
Cholest-22-ene-21-ol	7.2462	−7.58	5	1	1
cis-13-Octadecenoic acid	6.1085	−5.41	15	2	1
Hydroxycarbonate	0.36	−0.67	2	5	2
1-(4-(4-Methylphenyl)-5-phenyl-1,3-oxazol-2-yl)isoquinoline	3.74	−6.32	3	3	0

Swiss ADME and admetSAR servers were used to evaluate the metabolic properties of the identified SARS CoV-2 PLpro inhibitors. As shown in Table 3, most of the compounds obeyed Lipinski rules for drug-likeness [28]. Carbonoperoxoic acid has a molecular weight of 78.02 g/mol, log P of 0.154, four hydrogen bond acceptors (HBA) and two hydrogen bond donors (HBD).Chrysophanol-9-anthrone compound has a molecular weight of 240.25 g/mol, log P of 2.54, three HBA and two HBD atoms. Adrenolutin has a molecular weight of 179.17 g/mol, log P of 0.73, log S of −1.87, three HBA and two HBD. 1-Dehydroprogesterone has a molecular weight of 312.45 g/mol, log P of 4.49, log S of −4.28

and two HBA. Cholest-22-ene-21-ol has a molecular weight of 386.65 g/mol, log P of 7.25, log S of −7.58, 1 HBA and one HBD.Cis-13-Octadecenoic acid has a molecular weight of 282.46 g/mol, log P of 6.1, log S of −5.41, two HBA and one HBD. Hydroxycarbonate has a molecular weight of 9.402 g/mol,logP of 0.36, two Rotatable bonds, five HBA and two HBD. 1-(4-(4-Methylphenyl)-5-phenyl-1,3-oxazol-2-yl)isoquinoline has a molecular weight of 362.42g/mol, logP of 3.74, three rotatable bonds, three HBA and Zero HBD.

Other Pharmacokinetic properties such as absorption, distribution, metabolism, excretion and toxicity are presented in Table 4. The identified ligands are readily absorbed by the human intestine, making them good candidates for oral administration. Meanwhile, only Chrysophanol-9-anthrone and 1-Dehydroprogesterone could pass through the Blood-brain barrier.

Table 4. ADMET of the identified compounds.

Absorption and distribution	Ligand 1	Ligand 2	Ligand 3	Ligand 4	Ligand 5	Ligand 6	Ligand 7	Ligand8
Water solubility	Very soluble	Moderately	Very soluble	Moderate	Poor	Moderate	Very soluble	Poorly soluble
Blood-brain barrier permeant	No	Yes	No	Yes	No	No	No	Yes
Human intestinal absorption	High	High	High	High	High	High	High	High
CNS permeability	No	No	No	No	No	No	No	No
P-glycoprotein I inhibitor	No	No	No	Yes	Yes	No	No	No
P-glycoprotein II inhibitor	No	No	No	No	Yes	No	No	No
Metabolism								
CYP450 2C9 inhibitors	No	No	No	yes	No	No	No	No
CYP450 2D6 inhibitors	No	No	No	No	No	No	No	No
CYP450 3A4 substrate	No	No	No	yes	Yes	yes	No	Yes
CYP450 1A2 substrate	No	yes	No	No	No	yes	No	Yes
CYP450 2C19 inhibitors	No	yes	No	No	No	No	No	Yes
Toxicity								
AMES toxicity	No	No	No	No	No	No	No	No
hERG I inhibitor	No	No	No	No	No	No	No	No
hERG II inhibitor	No	No	No	Yes	Yes	No	No	No
Hepatotoxicity	No	No	No	Yes	No	Yes	No	No

Note: Ligand 1: Carbonoperoxoic acid, Ligand 2: Chrysophanol-9-anthrone, Ligand 3: Adrenolutin, Ligand 4: 1-dehydroprogesterone, Ligand 5: Cholest-22-ene-21-ol, Ligand 6: cis-13-Octadecenoate acid, Ligand 7: Hydroxycarbonate, Ligand 8: 1-(4-(4-Methylphenyl)-5-phenyl-1,3-oxazol-2-yl)isoquinoline.

4. Discussion

With the recent advancement in computational chemistry, chemical libraries could be screened for compounds with the potential to be utilized for drug development [17,29]. Several researchers have screened various chemical libraries in an attempt to discover potent PLpro inhibitors [15,16]. PLpro plays an essential role in the cleavage and maturation of SARS-CoV-2 poly-proteins, assembly of the replicase-transcriptase complex and disruption of host responses. The enzyme performs its proteolytic functions through its catalytic cysteine-protease cycle, in which Cys111 functions as a nucleophile, His272 acts as a general acid/base, and Asp286, linked with the histidine, assists to align and deprotonate Cys111 [5,6]. Several important structural features dictate access to the PLpro narrow active site, including a series of loops surrounding the area. One such loop is situated at the active site's mouth and comprises residues 103–110 [30]. As such, it is difficult for chemical compounds to fit the active site of SARS-CoV-2 PLpro. However, our study revealed that some of the identified compounds have the potential to bind to the SARS-CoV-2 PLpro catalytic triad and form crucial hydrogen bonds with catalytically essential residues of the enzyme and possibly inhibit its catalytic activity. For instance, carbonoperoxoic acid, cis-13-Octadecenoic acid, Hydroxycarbonate and 1-(4-(4-Methylphenyl)-5-phenyl-1,3-oxazol-2-yl)isoquinoline interacted with at least one of the active site catalytic triad residues of SARS-CoV-2 PLpro. More importantly, hydrogen bonds were formed between Carbonoperoxoic acid and Asp286, Ile285 and Tyr 273, while cis-13-Octadecenoic acid formed hydrogen bonds with Cys111 and Asn110. Hydroxycarbonate forms three hydrogen bonds with His 275, Ser 103 and Ile 285, and van der Waals interactions with catalytic Cys111 and Asp286. On the other hand, 1-(4-(4-Methylphenyl)-5-phenyl-1,3-oxazol-2-yl) isoquinoline forms a Pi-cation bond with Asp 286, Pi-anion bond with Lys 274 and Pi-donor hydrogen bond with Trp 106, which are all critical for the enzyme activity. On the other hand, adrenolutin binds to the pocket in the ubiquitin-binding domain and forms key hydrogen bonds with His 175, Ala 153, Arg 82 and Asn 156. Recent in-vitro studies imply that PLpro inhibitors that bind to the active or ubiquitin-binding sites are promising candidates for drug development [6]. In similar studies, Debnath et al. identified myricetin from Allium cepa and α-hydroxy-hydro-caffeic acid from Mentha piperita, both of which interacted with the SARS-Cov-2 PLpro [31].

Furthermore, several new molecules with anti-Covid-19 properties were identified by in silico studies, most of which are comparable to our findings. For instance, Hajbabaie et al. conducted a virtual screening of more than 300 thousand ligands and identified two compounds with binding scores of −9.4 and −9.36 kcal/mol which interacted with Asp 164, Glu 269, Tyr 264 and Tyr 268.

Similarly, a known PLpro inhibitor GLR0617 binds to the cavity near catalytic residues and induces the blockage of loop2, thereby preventing catalysis as observed in adrenolutin interaction[16]. An in-vitro study confirmed that a naphthalene-based compound identified by in silico studies has anti-PLpro activity [15]. Likewise, through virtual screening and enzymatic evaluations, nine natural biflavones were confirmed to be effective PLpro inhibitors with IC50 values ranging from 9.5 to 43.2 μM [32]. Adam et al. identified a compound that formed a hydrogen bond with Gly 163 and Alkyl interaction with Cys 111 and Leu 162 [33].

In our study, molecular dynamics simulation revealed that all the selected compounds formed a stable complex with SARS-CoV-2 PLpro. Similarly, MMPBSA revealed significant binding energies of the

complexes. Cholest-22-ene-21-ol showed the highest binding energy, followed by 1-Dehydroprogesterone, while Cis-13-Octadecenoic acid has the least binding energy.Metabolic and toxicity studies show that the identified compounds were all soluble and highly absorbed through the human intestine. Only Chrysophanol-9-anthrone and1-Dehydro progesterone are permeable to the blood-brain barrier (Table 4). Several studies revealed the therapeutic potential of the identified chemical compounds. For instance, Chrysophanol, which is a unique anthraquinone,has broad-spectrum therapeutic potential. It has been reported to possess anticancer, antiviral, anti-diabetic, anti-inflammatory and anti-protozoal effects [17]. Cholest-22-ene-21-ol has been reported to have an anti-inflammatory effect [34].Cis-13-octadecenoic acid is used for therapeutic uses in medicine and surgery [35], and Hydroxycarbonate is used in the synthesis of iron-magnesium-hydroxycarbonate for the treatment of hyperphosphatemia [36]. 1-(4-(4-Methylphenyl)-5-phenyl-1,3-oxazol-2-yl)isoquinoline modulates signal transduction through the Pd-1 receptor, which activates t-cells to promote immune response for treating infections, as reported in PubChem bioassay result.

5. Conclusions

Covid-19 remains the most significant challenge facing the world today, and so far, there is no standard therapeutic for its management. PLpro plays a critical role in viral replication and pathogenesis. Our present study has identified eight compounds, some of which form bonds with at least one of the catalytic triads of the PLpro, which is often difficult to achieve due to the presence of critical structural features that dictate access to the PLpro narrow active site. These ligands might have antiviral properties and the capacity to be promising drug candidates for the treatment of Covid-19. Furthermore, these compounds warrant further lead optimization and in-vitro studies.

Conflict of interest

The authors declare no conflict of interest.

Author contributions

MM, IYH and DL: conceptualization, methodology, writing of the original draft, editing and reviewing; AY, AJA and SYI: writing of the original draft, methodology; TAM, AJ and HS: methodology and writing of the original draft. All authors have read and approved the manuscript.

References

1. Hilgenfeld R (2014) From SARS to MERS: crystallographic studies on coronaviral proteases enable antiviral drug design. FEBS J 18: 4085–4096. https://doi.org/10.1111/febs.12936

2. Singhal T (2020) A review of coronavirus disease-2019 (COVID-19). Indian J Pediatr 87: 281–286. https://doi.org/10.1007/s12098-020-03263-6

3. Aftab SO, Ghouri MZ, Masood MU, et al. (2020) Analysis of SARS-CoV-2 RNA-dependent RNA polymerase as a potential therapeutic drug target using a computational approach. J Transl Med 18: 275. https://doi.org/10.1186/s12967-020-02439-0

4. ul Qamar MT, Alqahtani SM, Alamri MA, et al. (2020) Structural basis of SARS-CoV-2 3CLpro and anti-COVID-19 drug discovery from medicinal plants. J Pharm Anal 10: 313–319. https://doi.org/10.1016/j.jpha.2020.03.009

5. Gao X, Qin B, Chen P, et al. (2021) Crystal structure of SARS-CoV-2 papain-like protease. Acta Pharm Sin B 11: 237–245. https://doi.org/10.1016/j.apsb.2020.08.014

6. Osipiuk J, Azizi SA, Dvorkin S, et al. (2021) Structure of papain-like protease from SARS-CoV-2 and its complexes with non-covalent inhibitors. Nat Commun 12: 743.

7. Mielech AM, Chen Y, Mesecar AD, et al. (2014) Nidovirus papain-like proteases: multifunctional enzymes with protease, deubiquitinating and deISGylating activities. Virus Res194: 184–190. https://doi.org/10.1016/j.virusres.2014.01.025

8. Lindner HA, Lytvyn V, Qi H, et al. (2007) Selectivity in ISG15 and ubiquitin recognition by the SARS coronavirus papain-like protease. Arch Biochem Biophys 466: 8–14. https://doi.org/10.1016/j.abb.2007.07.006

9. Swaim CD, Canadeo LA, Monte KJ, et al. (2020) Modulation of extracellular ISG15 signaling by pathogens and viral effector proteins. Cell Rep 31: 107772. https://doi.org/10.1016/j.celrep.2020.107772

10. Barretto N, Jukneliene D, Ratia K, et al. (2005) The papain-like protease of severe acute respiratory syndrome coronavirus has deubiquitinating activity. J Virol 79: 15189–15198. https://doi.org/10.1128/JVI.79.24.15189-15198.2005

11. Klemm T, Ebert G, Calleja DJ, et al. (2020) Mechanism and inhibition of the papain-like protease, PLpro, of SARS-CoV-2. EMBO J 39: e106275. https://doi.org/10.15252/embj.2020106275

12. Chojnacka K, Witek-Krowiak A, Skrzypczak D, et al. (2020) Phytochemicals containing biologically active polyphenols as an effective agent against Covid-19-inducing coronavirus. J Funct Foods 73: 104146. https://doi.org/10.1016/j.jff.2020.104146

13. Alamri MA, Tahir Ul Qamar M, Mirza MU, et al. (2021) Pharmacoinformatics and molecular dynamics simulation studies reveal potential covalent and FDA-approved inhibitors of SARS-CoV-2 main protease 3CLpro. J Biomol Struct Dyn 39: 4936–4948. https://doi.org/10.1080/07391102.2020.1782768

14. Oladele JO, Adewole TS, Ogundepo GE, et al. (2022) Efficacy of selected Nigerian tropical plants in the treatment of COVID-19: in silico and in vitro investigations. Environ Sci Pollut Res29: 627. https://doi.org/10.1007/s11356-022-22025-9

15. Yan F, Gao F (2021) An overview of potential inhibitors targeting non-structural proteins 3 (PLpro and Mac1) and 5 (3CLpro/Mpro) of SARS-CoV-2. Comput Struct Biotechnol J 19: 4868–4883. https://doi.org/10.1016/j.csbj.2021.08.036

16. Hajbabaie R, Harper MT, Rahman T (2021) Establishing an analogue based in silico pipeline in the pursuit of novel inhibitory scaffolds against the SARS coronavirus 2 papain-like protease. Molecules 26: 1134. https://doi.org/10.3390/molecules26041134

17. Yadav JP, Arya V, Yadav S, et al. (2010) Cassia occidentalis L.: a review on its ethnobotany, phytochemical and pharmacological profile. Fitoterapia 81: 223–230. https://doi.org/10.1016/j.fitote.2009.09.008

18. Socrates SH, Mohan SC (2019) Phytochemical analysis of flower extracts of different Cassia species by using gas chromatography-mass spectrometry. Int J Biol Chem 13: 1–11.

19. Manikandaselvi S, Vadivel V, Brindha P, et al. (2016) Studies on physicochemical and nutritional properties of aerial parts of Cassia occidentalis L. J Food Drug Anal 24: 508–515. https://doi.org/10.1016/j.jfda.2016.02.003

20. Mirza MU, Froeyen M (2020) Structural elucidation of SARS-CoV-2 vital proteins: Computational methods reveal potential drug candidates against main protease, Nsp12 polymerase and Nsp13 helicase. J Pharm Anal 10: 320–328. https://doi.org/10.1016/j.jpha.2020.04.008

21. Pettersen EF, Goddard TD, Huang CC, et al. (2004) UCSF Chimera—a visualization system for exploratory research and analysis. J Comput Chem 25: 1605–1612. https://doi.org/10.1002/jcc.20084

22. Pronk S, Páll S, Schulz R, et al. (2013) GROMACS 4.5: a high-throughput and highly parallel open source molecular simulation toolkit. Bioinformatics 29: 845–854. https://doi.org/10.1093/bioinformatics/btt055

23. Vanommeslaeghe K, Hatcher E, Acharya C, et al. (2010) CHARMM general force field: a force field for drug-like molecules compatible with the CHARMM all-atom additive biological force fields. J Comput Chem 31: 671–690. https://doi.org/10.1002/jcc.21367

24. Genheden S, Ryde U (2015) The MM/PBSA and MM/GBSA methods to estimate ligand-binding affinities. Expert Opin Drug Discov 10: 449–461. https://doi.org/10.1517/17460441.2015.1032936

25. Kumari R, Kumar R, Consortium OSDD, et al. (2014) g_mmpbsa–A GROMACS tool for high-throughput MM-PBSA calculations. J Chem Inf Model 54: 1951–1962. https://doi.org/10.1021/ci500020m

26. Miller III BR, McGee Jr TD, Swails JM, et al. (2012) MMPBSA. py: an efficient program for end-state free energy calculations. J Chem Theory Comput 8: 3314–3321. https://doi.org/10.1021/ct300418h

27. Cheng F, Li W, Zhou Y, et al. (2012) admetSAR: a comprehensive source and free tool for assessment of chemical ADMET properties. J Chem Inf Model 52: 3099–3105. https://doi.org/10.1021/ci300367a

28. Ntie-Kang F (2013) An in silico evaluation of the ADMET profile of the StreptomeDB database.Springerplus 2: 353. https://doi.org/10.1186/2193-1801-2-353

29. Sofowora A, Ogunbodede E, Onayade A, et al. (2013) The role and place of medicinal plants in the strategies for disease prevention. Afr J Tradit Complement Altern Med 10: 210–229. https://doi.org/10.4314/ajtcam.v10i5.2

30. Ratia K, Saikatendu KS, Santarsiero BD, et al. (2006) Severe acute respiratory syndrome coronavirus papain-like protease: structure of a viral deubiquitinating enzyme. Proc Natl Acad Sci 103: 5717–5722. https://doi.org/10.1073/pnas.0510851103

31. Debnath B, Debnath P, Ghosh R, et al. (2021) In silico identification of potential inhibitors of SARS-CoV-2 papain-like protease from natural sources: A natural weapon to fight COVID-19. Coronaviruses 2: 16–27. https://doi.org/10.2174/2666796701999201203211330

32. Li L, Ma L, Hu Y, et al. (2022) Natural biflavones are potent inhibitors against SARS-CoV-2 papain-like protease. Phytochemistry 193: 112984. https://doi.org/10.1016/j.phytochem.2021.112984

33. Stasiulewicz A, Maksymiuk AW, Nguyen ML, et al. (2021) SARS-CoV-2 papain-like protease potential inhibitors—in silico quantitative assessment. Int J Mol Sci 22: 3957. https://doi.org/10.3390/ijms22083957

34. Johnson TO, Odoh KD, Nwonuma CO, et al. (2020) Biochemical evaluation and molecular docking assessment of the anti-inflammatory potential of Phyllanthus nivosus leaf against ulcerative colitis. Heliyon 6: e03893. https://doi.org/10.1016/j.heliyon.2020.e03893

35. Astiti NPA, Ramona Y (2021) GC-MS analysis of active and applicable compounds in methanol extract of sweet star fruit (Averrhoa carambola L.) leaves. HAYATI J Biosci 28: 12–12. https://doi.org/10.4308/hjb.28.1.12

36. McIntyre CW, Pai P, Warwick G, et al. (2009) Iron-magnesium hydroxycarbonate (fermagate): a novel non-calcium-containing phosphate binder for the treatment of hyperphosphatemia in chronic hemodialysis patients. Clin J Am Soc Nephrol 4: 401–409. https://doi.org/10.2215/CJN.02630608

Effect of Rs5746136 genotypes on SOD activity and biomarkers levels in breast cancer patients

Hadi Sajid Abdulabbas1 and Yasir Haider Al-Mawlah2,*

1 Continuous Education Department, Faculty of Dentistry, University of Al-Ameed, Karbala, 56001, Iraq

2 DNA Research Center, University of Babylon, Babylon, Hillah-Najaf Street, 51001, Iraq

ABSTRACT

Oxidative stress factors are among the most common carcinogens, Superoxide dismutase enzyme-2 (SOD2) is an endogenous antioxidant involved in the scavenging of superoxide anions. This study aimed to investigate the effect of the SOD2 gene polymorphism (rs5746136) on SOD activity and biomarker levels in breast cancer patients. This study aimed to investigate the effect of SOD2 gene (rs5746136) polymorphisms on SOD activity and biomarkers levels in breast cancer patients. The spectrophotometry methods were used to detect malondialdehyde (MDA) and Catalase (CAT), Superoxide dismutase (SOD), and Glutathione (GSH) levels, which reflect antioxidant capacity, and the genotypes of rs5746136 were detected utilize PCR and RFLP. According to the current findings, the GA genotype of the control group was the most common (70%), followed by GG and AA genotypes (26.7% and 3.3%) respectively. In the patient group, the most common genotype was GG (45.6%), followed by the GA genotype (42.8%) and then the AA genotype (11.4%) The frequency of heterozygous genotype G/A compared to the homozygous genotype (G/G) [OR = 0.3571, 95% CI = 0.1375–0.9277, P = 0.0345]. The AA genotype is significantly associated with an increased risk of developing BC [OR = 2.00, p = 0.5403, CI: 0.2175–18.3883]. No significant differences were found in frequencies of the A allele between patients and control groups [OR = 0.7872, 95% CI = 0.4198–1.4762, P = 0.4558]. In addition, there are modest (P 0.05) relationships between serum biochemical parameters levels and rs5746136 genotype in breast cancer patients, but a substantial association between serum SOD activity and GSH concentration and GA and GG rs5746136 genotype in the control group. In conclusion, the current investigation suggests that the AA genotype of (rs5746136) in the MnSOD gene may be associated with an increased risk of breast cancer. The chosen SOD2 variants (rs5746136) play a crucial role in controlling the activity of the SOD enzyme.

Keywords: breast cancer; antioxidant polymorphism; MnSOD; Rs5746136; SOD2; RFLP-PCR

1. Introduction

The most common cancer among women is breast cancer (one-third of all female cancers), it is the second-highest cancer-causing death after lung cancer and the first on the list causing death in American women between 40–55 years old [1]. In general, the accumulation of damaged DNA affects signal transduction pathways within cells, and oxidative stresses are the main factors that cause cancer development [2]. Reactive oxygen species have been linked to the emergence of cancer in numerous well-established research (ROS). One of their most notable known traits is that they are extremely reactive, created by various diseases, pharmaceutical medications, UV radiation, and ROS-trigger inflammatory cells.

ROS are considered inducers of malignancy because they can promote the transformation of oncogenes and increase cell proliferation, survival, and migration due to the accumulation of damaged DNA. Oxidative stress increases when the body produces ROS and cannot remove them effectively, which can cause serious health problems [3–5]. Superoxide dismutase (SOD), which is found in the mitochondria, peroxisomes, and cytoplasm, is the body's main ROS-activated antioxidant defense system [3,6]. SOD enzyme catalyzes the dismutation of superoxide into oxygen and hydrogen peroxide [7–9]. Three families of superoxide dismutase are generated according to the type of metal cofactor: copper/zinc Cu/Zn (SOD1, OMIM No. 147450); ferritin/manganese Fe/Mn (SOD2, OMIM No. 147460); and nickel Ni (SOD3, OMIM No. 185490) [10]. The increased or decreased activity of antioxidant enzymes such as GPx, CAT, SOD, GST, and GR has become a significant and necessary tool for understanding the development of cancer and therapy [11]. Several studies have shown some indication that genetic variants in the MnSOD gene may be connected to an increased chance of breast cancer in Chinese women with high-rise levels of oxidative stress or reduced antioxidant consumption [7,11]. The mutations in the SOD2 gene are risk factors for tumor progression [12]. Several investigations have indicated the possibility of polymorphisms in the MnSOD gene, affecting gene expression and/or protein function, referring to the predicted relationship between SNPs in the enzyme gene and cancer development [1,2,13]. The rs5746136 C > T or G > A is associated with the development of premature [3], cardiovascular illnesses [4], diabetes mellitus type 2 (DM2) [5], and cancer [7,10,13], some of the variants are linked to reduced enzymatic activity. The rs5746136 variants are situated around one kilobase upstream from SP1 and the NF-kB transcription element sequences and 65 base pairs downstream of the poly-A site in the 5th intron, close to 3′UTR. The biological impact of the variations is unknown, but some theories have suggested that it may influence how genes are expressed, transport mRNA to the cytoplasm, and affect mRNA half-life. In the Chinese population, bladder cancer risk is correlated with genetic variations in N6-methyladenosine [11]. The SOD2 gene variant might limit BC susceptibility, but the association Educations that studied the rs5746136 variants and BC risk remain unknown. For this reason, we deliberate it important to govern the frequency of the rs5746136 variants, and whether there is a correlation between SOD2 gene polymorphisms and Iraqi women with BC.

2. Materials and methods

2.1. Ethical statements

Written consent forms have been given by volunteers. The University of Babylon's ethical committee accepted the study and authorized the collection of samples.

2.2. Population of study

The study included 70 patients with breast cancer at Merjan University Hospital aged a rounded 25–81 years old, the healthy control group consist of 30 healthy females (20–71 years old). Samples start collecting between September 2021 and January 2022. Every individual provided a written authentication.

2.3. Blood samples

About four milliliters of venous blood sample was collected from each subject in this study. Each blood sample was divided into two parts 2 ml for each: the first part was collected into EDTA containing tubes to use for genetic analysis, and the second part was used to separate the serum by centrifugation at 3000 rpm for 15 min and then kept in Eppendorf tubes at –20 °C until used [14,15]. 2.4. Biochemical analysis

2.4. Biochemical analysis

2.4.1. Superoxide dismutase (SOD) assay

According to [12], superoxide dismutase activities were assessed through Pyrogallol self oxidation. pyrogallol rapidly autoxidizes in the existence of molecular oxygen, in an alkaline medium, to produce numerous intermediate products. The principle of this procedure is based on the mass production of pyrogallol-quinone through a reactive intermediate, the semiquinone radical, and the capability of SOD to block this reaction by radical dismutation. Pyrogallol-quinone is nut brown and absorbs visible light at 420 nm. One unit of SOD activity is defined as the quantity of enzyme required to block the oxidation of pyrogallol autoxidation by 50% per min per ml of the assay combination.

2.4.2. Catalase (CAT) assay

Serum catalase activity was measured using hydrogen peroxide as a substrate assay based on forming a stable complex with ammonium molybdate [16,17]. The test for glutathione content was based on the formation of a yellow-colored compound by dithionitrobenzene (DTNB) with acidsoluble sulfhydryl groups, as described by [18].

2.4.3. Lipid peroxidation

Lipid peroxidation was estimated using the thiobarbituric acid assay for malondialdehyde (MDA) concentration based on [19]. Malondialdehyde (MDA), the main product of lipid peroxidation, and thiobarbituric acid (TBA) interact in the assay to create MDA-TBA2 adducts known as TBARS. A reddish-pink tint produced by TBARS can be observed spectrophotometrically at 532 nm.

2.5. Molecular assay

2.5.1. DNA extraction

Following the manufacturer's instructions, gDNA was extracted from blood samples using the Genomic DNA Mini Kit (Blood/Cultured Cell) (Catalog number GB100/300, Genaid, Taiwan). The absorbance at two wavelengths (260 and 280) on a (Nanophotometer NP80, Implen, Germany) at the Advanced Microbiology Lab, biology department, College of Science, University of Babylon, Babylon, Iraq, was used to assess the quality of the DNA sample. For subsequent tests, all DNA samples were maintained at a temperature of 20 °C [15,16,20].

2.5.2. Polymerase chain reaction (PCR)

DNA-targeted sites were amplified using a specifically designed primer to detect and recognize the MnSOD (rs5746136) gene (Macrogene, South Korea). Forward primer 5′-GATGCCTTTCTCCTATTC-3′ and the reverse primer was 5′-TCAGTCACCTGCTACATT-3′. The Polymerase Chain Reaction PCR technique was performed with a reaction volume of 20 µl (1 µl of each primer, 12.5 µl of green master mix, 3 µl of DNA, and 2.5 µl of DNase-free water. Amplification was carried out by thermal cycler (Biometra, Germany) as the following program: 95 °C for denaturation for 5 minutes, 35 cycles for 30 seconds at 94 °C, annealing for 25 seconds at 60 °C, extension for 30 seconds at 72 °C and final extension for 5 minutes.

The product of PCR was electrophorized in 1% agarose gel at 75 V (cleaver sciences, UK) and then observed by using ethidium bromide. Gel documentation system (Cleaver science-UK) used to capture photographs.

2.5.3. Polymerase chain reaction-restriction fragment length polymorphism (PCR-RFLP)

According to the manufacturer's instructions, the PCR product was digested by two units of candidate endonuclease TaqI for 14 hrs at 65 °C (Promega). PCR products were electrophorized with 1% agarose at 75 V (Cleaver science-UK) and stained with ethidium bromide for visualization.

2.6. Statistical analysis

The statistical analyses in this study were carried out using IBM SPSS statistics version 23.0. To compare sample means from two related groups, the dependent samples t-test is utilized. The whole number of incidences of the tested allele in the population was divided by the whole number of alleles to compute allele frequencies. The odds ratio (OR), 95% confidence intervals, and P values of the genotype distributions and allele frequencies were calculated using the Hardy-Weinberg equilibrium assumption and a Chi-square test. Duncan's test was used to investigate the correlation between blood biochemical parameter levels and rs1050450 genotypes. All $P < 0.05$ were considered statistically significant [21–23].

3. Results

As a preliminary step in amplifying the target area of the SOD1 gene, genomic DNA was isolated from Blood samples.

3.1. Genotyping of SOD2 (rs5746136) gene polymorphisms

The results of gene polymorphism show the presence of a unique band (253 bp) of the SOD2 gene target sequence (rs5746136).SOD2 (rs5746136) gene PCR products were digested by TaqI restriction enzyme which cut the sequence (5′TCG3′) to recognize rs2576178 SNP in the SOD2 gene as shown in Figure 1. Genotyping was classified into three categories according to presence/absence of polymorphism: G/G homozygote with two bands as 130 and 123 bp, G/A heterozygote with three bands as 253, 130, 123 bp, and AA homozygous with a single band as 253 bp.
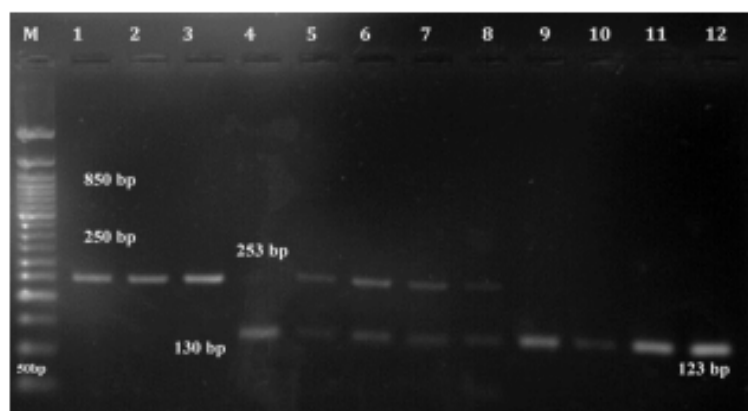
Figure 1. SOD2 gene (rs5746136) allelotyping in patients with breast cancer and healthy individuals depending on using TaqI restriction enzyme according to PCR-RFLP technique showed as follows: lane 1–3: present the AA homozygous allele as a single band of 253 bp, lane 5–8: refer to GA heterozygous allele as three bands of 253, 123, 130 bp, lane 4, 9–12: represent the GG homozygous allele as two bands of 130 and 123 bp.

3.2. The genotypes distribution of SOD2 rs5746136 polymorphisms with allele frequency in control and case groups

SOD2 gene (rs5746136) polymorphism distribution in study groups as shown in Table 1, the GA genotype (70%) was the greatest distributed in the control group, then the GG genotype (26.7%), followed by the mutant AA (3.3%). Instantly, the homozygote GG was the most common genotype (45.6%), then followed by the heterozygous GA genotype (42.8%), and mutant AA genotype (11.4%). The frequency of the G/A heterozygous genotype in comparison with the G/G homozygous genotype (OR: 0.3571, 95% CI: 0.1375–0.9277, P value: 0.0345). The AA allele of rs5746136 was remarkably associated with an increased chance of developing BC [OR = 2.00, p = 0.5403, CI: 0.2175–18.3883]. Polymorphism in the MnSOD2 (rs5746136) gene shows unimportant variations in allele A frequency among patients and the control group (OR: 0.7872, 95% CI: 0.4762, P value: 0.4558).

Table 1. Distribution of SOD2 (rs5746136) genotype and odd ratio among patients and control group.

Genotype rs5746136	Patients No. (%)	Control No. (%)	P-value	O. R	CI (95%)
GG[a]	32 (45.6%)	8 (26.7%)			
GA	30 (42.8%)	21 (70%)	0.0345	0.3571	0.1375–0.9277
AA	8 (11.4%)	1 (3.3%)	0.5403	2.0000	0.2175–18.3883
Total No.	70 (100%)	30 (100%)			
Allele	Frequency	Frequency			
G	0.67	0.61			
A	0.33	0.39	0.4558	0.7872	0.4198–1.4762

$P \leq 0.05$; OR = (95% CI); [a] reference.

The current findings revealed that the SOD2 (rs5746136) AA and GA genotypes promote a decrease in SOD activity (40.037129.62) U/ml and (40.037129.62) U/ml, respectively. GSH, MDA levels, and CAT activity were not altered in BC patients. Furthermore, as listed in Table 2, the GA genotype reduces SOD activity (51.588630.42) U/ml in the healthy control group.

Table 2. Biochemical parameters levels in association with SOD2 (rs5746136) genotype.

Group	Genotype of SOD2 (rs5746136)	Mean ± SD SOD activity	GSH	CAT activity	MDA
Patients	AA	40.0371 ± 29.62a	6.1871 ± 4.64a	11.964 ± 11.21a	1.467 ± 1.014a
	GA	40.3042 ± 22.38a	7.7625 ± 6.3533a	9.5076 ± 5.693a	1.561 ± 1.380a
	GG	42.2578 ± 24.72b	8.5037 ± 7.2248a	9.4274 ± 3.9164a	1.476 ± 1.168a
Control	AA	29.4433a	20.1317a	8.0887a	1.1083a
	GA	51.5886 ± 30.42a	13.2198 ± 12.54a	17.1516 ± 7.905a	1.84 ± 1.585a
	GG	63.5457 ± 22.14b	19.2335 ± 12.52a	17.5300 ± 9.772a	2.07 ± 0.6787a

4. Discussion

Contrasting theories have been proposed regarding the function of the SOD2 enzyme in the modulation of oxidative stress that ROS generates (tumor promoter) in the cell and the progress of cancer. Furthermore, the SOD2 gene has binding sites for disparate transcription elements thatbehave as a ligand to activate the transcription and participate as a cell defense system as opposed to agents that persuade oxidative stress [7,24]. Studies linking the SOD2 rs5746136 variation to BC have revealed a variety of susceptibilities, including those associated with risk

[25,26], some with protection [27], and still others without a connection [14,28]. The relationship between the SOD2rs5746136 variations and BC susceptibility in the Iraqi population is not well understood, yet. In the current investigation, there were statistically significant differences between BC patients and controls in the frequency of the GA and AA genotypes of the SOD2 rs5746136 variations, which were linked to an increased risk of developing BC ($p < 0.05$).

This is the first study to investigate the relationship between SOD2 rs5746136 variations and BC in the Iraqi population. When compared to the wild-type homozygous genotype, variation in the A allele of the MnSOD genotype was found to have a 2-fold (0.2175–18.3883 percent CI) greater risk of breast cancer. The findings presented in the current study credibly support the idea that MnSOD genotypes may influence breast cancer risk [15]. In this instance, numerous studies have examined the expression of SOD2 in BC; nonetheless, it is still unclear how BC is regulated to develop. T alleles from SOD2 (rs5746136) changes are likely to alter the inadequate activity of the SOD2 enzyme. The cellular defense systems and antioxidant defense capabilities are hence ineffective. Gene regulatory pathways can foresee and start the development of BC because oxidative stress is produced [29].

Many other studies linked the A/a genotype form to increased risk of cancer, like bladdercancer, Gastric Cancer, and primary open angle glaucoma [15,30,31]. With the help of this information, it can be concluded that the AA genotype of the rs5746136 variant confers a favorable susceptibility to BC. On the other hand, the development of cancer is complex and depends on interactions between various genes engaged in various metabolic pathways, epigenetic processes, and environmental variables rather than just being tied to the monogenic inheritance of a protein variant [32,33]. There was a study revealed that the rs-4880 and rs-4244285 and rs1001179 polymorphisms also play a crucial role in breast cancer development in the Iraqi population, but the rs-1801274 and rs2070424 wereshown an insignificant association with the risk of breast cancer [25,34].

The study looked at selected variants in SOD2 30UTR A > G (rs5746136), genes that have previously been identified as having essential roles in the control of the oxidative stress process. MnSOD2 (rs5746136) gene is situated 65 bp downstream of the poly-A tail site in the 3′UTR of the SOD2 gene. Also, about 1kbp upstream of the NF-B and SP1 transcription factors sequences [35]. Because of environmental factors [36–38], and polymorphism in regulatory areas of the genes [39].affected the expression levels of the superoxide dismutase family members, including SOD2, in this situation, they may play key roles. The positions of the rs5746136 suggest that these genetic variations are probably capable of controlling the expression of the SOD2 gene. We, therefore,proposed the possibility that these genetic variants could be linked to the risk of BC.Previous research suggested that these polymorphisms were linked to the risks of multifactorial features related to oxidative stress [40,41]. The AA genotype of rs5746136 variants increased with the risk of heroin addiction and the haplotype AA was associated with the increase in heroin addiction, there was no correlation between genotype studies and the level of SOD2 expression [42].

There are several limitations to this study. First, the SOD2 gene contains a variety of other polymorphisms. Further study of the impact of SOD2 polymorphisms on mRNA levels should be conducted concurrently. Second, it has been noted that certain environmental factors, such as electromagnetic fields and medications, are linked to the mRNA levels of some antioxidant genes (such as catalase, SOD2, SOD1, etc.) [43]. More study with bigger sample numbers is needed to confirm the role of the rs5746136 polymorphisms in the pathophysiology of BC.

5. Conclusions

This study found that the AA genotype in the MnSOD gene (rs5746136) was associated with a higher risk of breast cancer than the GG and GA genotypes. The MnSOD2 gene variation is crucial in

modulating SOD enzyme activity, which can lead to uncontrolled ROS and oxidative stress, which is one of the stimulation and risk factors for cancer formation. The rs5746136 variant is located in the 5th intron and has the potential to affect gene transcription, RNA splicing, and mRNA half-life.

Conflict of interest
The authors declare no conflict of interest.

References

1. Glynn SA, Boersma BJ, Howe TM, et al. (2009) A mitochondrial target sequence polymorphism in manganese superoxide dismutase predicts inferior survival in breast cancer patients treated with cyclophosphamide. Clin Cancer Res 15: 4165–4173. https://doi.org/10.1158/1078-0432.CCR-09-0119

2. Barretina J, Caponigro G, Stransky N, et al. (2012) The cancer cell line encyclopedia enables predictive modelling of anticancer drug sensitivity. Nature 483: 603–607. https://doi.org/10.1038/nature11003

3. Soerensen M, Christensen K, Stevnsner T, et al. (2009) The Mn-superoxide dismutase single nucleotide polymorphism rs4880 and the glutathione peroxidase 1 single nucleotide polymorphism rs1050450 are associated with aging and longevity in the oldest old. Mech Ageing Dev 130: 308–314. https://doi.org/10.1016/j.mad.2009.01.005

4. Yari A, Saleh-Gohari N, Mirzaee M, et al. (2022) A study of associations between rs9349379 (PHACTR1), rs2891168 (CDKN2B-AS), rs11838776 (COL4A2) and rs4880 (SOD2) polymorphic variants and coronary artery disease in Iranian population. Biochem Genet 60: 106–126. https://doi.org/10.1007/s10528-021-10089-0

5. Ascencio-Montiel IDJ, Parra EJ, Valladares-Salgado A, et al. (2013) SOD2 gene Val16Ala polymorphism is associated with macroalbuminuria in Mexican Type 2 Diabetes patients: a comparative study and meta-analysis. BMC Med Genet 14: 110. https://doi.org/10.1186/1471-2350-14-110

6. Huober J, Schneeweiss A, Hartkopf AD, et al. (2020) Update breast cancer 2020 Part 3—early breast cancer. Obstet Gynecol 80: 1105–1114. https://doi.org/10.1055/a-1270-7208

7. Alateyah N, Gupta I, Rusyniak RS, et al. (2022) SOD2, a potential transcriptional target underpinning CD44-promoted breast cancer progression. Molecules 27: 811. https://doi.org/10.3390/molecules27030811

8. Frederiks WM, Bosch KS, Hoeben KA, et al. (2010) Renal cell carcinoma and oxidative stress: the lack of peroxisomes. Acta Histochem 112: 364–371. https://doi.org/10.1016/j.acthis.2009.03.003

9. Gallegos-Arreola MP, Ramírez-Hernández MA, Figuera LE, et al. (2020) The rs2234694 and 50 bp insertion/deletion polymorphisms of the SOD1 gene are associated with breast cancer risk in a Mexican population. Eur Rev Med Pharmaco 24: 8017–8027.

10. Romero-Cordoba SL, Salido-Guadarrama I, Rebollar-Vega R, et al. (2021) Comprehensive omic characterization of breast cancer in Mexican-Hispanic women. Nat Commun 12: 2245. https://doi.org/10.1038/s41467-021-22478-5

11. Lemus-Varela ML, García-Valdez LM, Ramírez-Patiño R, et al. (2021) Association of the SOD2Rs5746136 C > T polymorphisms with the risk of persistent pulmonary hypertension of the newborn. J Pediatr Neonatal 3: 1–5.

12. Marklund S, Marklund G (1974) Involvement of the superoxide anion radical in the autoxidation of pyrogallol and a convenient assay for superoxide dismutase. Eur J Biochem 47: 469–474. https://doi.org/10.1111/j.1432-1033.1974.tb03714.x

13. Rendic S, Peter Guengerich F (2012) Summary of information on the effects of ionizing and non-ionizing radiation on cytochrome P450 and other drug metabolizing enzymes and transporters. *Curr Drug Metab* 13: 787–814. https://doi.org/10.2174/138920012800840356

14. Chen Y, Pei J (2011) Possible risk modifications in the association between MnSOD Ala-9Val polymorphism and breast cancer risk: subgroup analysis and evidence-based sample size calculation for a future trial. *Breast Cancer Res Tr* 125: 495–504. https://doi.org/10.1007/s10549-010-0978-9

15. Mitrunen K, Sillanpää P, Kataja V, et al. (2001) Association between manganese superoxide dismutase (MnSOD) gene polymorphism and breast cancer risk. *Carcinogenesis* 22: 827–829. https://doi.org/10.1093/carcin/22.5.827

16. Nawab SN, Zehra S, Fawwad A, et al. (2017) A study on catalase gene promoter polymorphism21 A/T (rs7943316) in healthy pakistani population. *Pak J Med Sci* 33: 1521–1524. https://doi.org/10.12669/pjms.336.13188

17. Borgstahl GEO, Parge HE, Hickey MJ, et al. (1996) Human mitochondrial manganese superoxide dismutase polymorphic variant Ile58Thr reduces activity by destabilizing the tetrameric interface. *Biochemistry-US* 35: 4287–4297. https://doi.org/10.1021/bi951892w

18. Moron MS, Depierre JW, Mannervik B (1979) Levels of glutathione, glutathione reductase and glutathione S-transferase activities in rat lung and liver. *BBA-Gen Subjects* 582: 67–78. https://doi.org/10.1016/0304-4165(79)90289-7

19. Garcia-Moreno C, Heise L, Jansen HAFM, et al. (2005) Violence against women. *Science* 310: 1282–1283. https://doi.org/10.1126/science.1121400

20. Al-Mawlah YH, Naji MZ, Al-Imari MJ, et al. (2022) Micro-RNA evaluation, specification, and stabilization study in mixed/non-mixed body fluids as a specific molecular marker. *J Adv Biotechnol Exp Ther* 5: 347–357. https://doi.org/10.5455/JABET.2022.D120

21. Al-Kashwan TA, Algenabi AHA, Omara AM, et al. (2021) Association of vitamin D receptor gene polymorphisms BsmI (rs 1544410) and TaqI rs (731236) with the type 2 diabetes mellitus in Iraqi patients from the middle Euphrates region. *Meta Gene* 28: 100854. https://doi.org/10.1016/j.mgene.2021.100854

22. Kaftan AN, Hussain MK, Algenabi AHA, et al. (2021) Association of sunshine vitamin receptor gene polymorphisms (rs2228570) and (rs7975232) with the type 2 diabetes mellitus in Iraqi patients from the middle Euphrates region. *Gene Rep* 22: 100977. https://doi.org/10.1016/j.genrep.2020.100977

23. Kocabaş NA, Şardaş S, Cholerton S, et al. (2005) Genetic polymorphism of manganese superoxide dismutase (MnSOD) and breast cancer susceptibility. *Cell Biochem Funct* 23: 73–76. https://doi.org/10.1002/cbf.1128

24. Hashim AM, Al-Harbi SJ, Burhan MM, et al. (2023) Histological and physiological determinants of hypothyroidism in patients and its relationship with lipid profile. *J Adv Biotechnol Exp Ther* 6: 9–16. https://doi.org/10.5455/jabet.2023.d101

25. Jabir FA, Hoidy WH (2018) Pharmacogenetics as personalized medicine: Association investigation of SOD2 rs4880, CYP2C19 rs4244285, and FCGR2A rs1801274 polymorphisms in a breast cancer population in Iraqi women. *Clin Breast Cancer* 18: e863–e868. https://doi.org/10.1016/j.clbc.2018.01.009

26. Kinnula VL, Crapo JD (2004) Superoxide dismutases in malignant cells and human tumors. *Free Radical Bio Med* 36: 718–744. https://doi.org/10.1016/j.freeradbiomed.2003.12.010

27. Tengström M, Mannermaa A, Kosma VM, et al. (2014) MnSOD rs4880 and XPD rs13181 polymorphisms predict the survival of breast cancer patients treated with adjuvant tamoxifen. *Acta Oncol* 53: 769–775. https://doi.org/10.3109/0284186X.2014.892210

28. Kakkoura MG, Demetriou CA, Loizidou MA, et al. (2016) MnSOD and CAT polymorphisms

modulate the effect of the Mediterranean diet on breast cancer risk among Greek-Cypriot women. *Eur J Nutr* 55: 1535–1544. https://doi.org/10.1007/s00394-015-0971-5

29. Hecht F, Pessoa CF, Gentile LB, et al. (2016) The role of oxidative stress on breast cancer development and therapy. *Tumor Biol* 37: 4281–4291. https://doi.org/10.1007/s13277-016-4873-9

30. Zhang Y, Zhang C, Guan S, et al. (2017) Association between SOD2 rs6917589, rs2842980, rs5746136 and rs4880 polymorphisms and primary open angle glaucoma in a northern Chinese population. *Int J Clin Exp Pathol* 10: 3930–3938.

31. Cengiz M, Ozaydin A, Ozkilic AC, et al. (2007) The investigation of GSTT1, GSTM1 and SOD polymorphism in bladder cancer patients. *Int Urol Nephrol* 39: 1043–1048. https://doi.org/10.1007/s11255-007-9179-9

32. Liu H, Gu J, Jin Y, et al. (2021) Genetic variants in N6-methyladenosine are associated with bladder cancer risk in the Chinese population. *Arch Toxicol* 95: 299–309. https://doi.org/10.1007/s00204-020-02911-2

33. Saify K, Saadat M (2015) Expression patterns of antioxidant genes in human SH-SY5Y cells after treatment with methadone. *Psychiat Res* 230: 116–119. https://doi.org/10.1016/j.psychres.2015.08.027

34. Al-Mawlah YH, Al-Darraji MN, Al-Imari MJ (2022) Study of small non-coding RNA (miRNA) expression pattern of fertile/infertile male semen. *Acta Inform Med* 30: 205–212. https://doi.org/10.5455/aim.2022.30.205-212

35. Wiener HW, Perry RT, Chen Z, et al. (2007) A polymorphism in SOD2 is associated with development of Alzheimer's disease. *Genes Brain Behav* 6: 770–776. https://doi.org/10.1111/j.1601-183X.2007.00308.x

36. Mahmoudinasab H, Saadat M (2016) Short-term exposure to 50-Hz electromagnetic field and alterations in NQO1 and NQO2 expression in MCF-7 cells. *Open Access Maced J Med Sci* 4: 548–550. https://doi.org/10.3889/oamjms.2016.102

37. Saify K (2016) Genetic polymorphisms in the promoter region of catalase gene, creates new potential PAX-6 and STAT4 response elements. *Mol Biol Res Commun* 5: 97–100.

38. Saify K, Saadat M (2017) Influence of a 50bp Ins/Del polymorphism at promoter of the superoxide dismutase-1 on gene expression and risk of heroin dependency. *Environ Health Prev* 22: 4. https://doi.org/10.1186/s12199-017-0617-8

39. Al-Mawlah YH, Alasadi YF, Al-Darraji MN (2021) Association between genetic polymorphisms of (Cu/ZnSOD and CAT C262T) and the risk of breast cancer. *Gene Rep* 25: 101401. https://doi.org/10.1016/j.genrep.2021.101401

40. Liu Y, Zha L, Li B, et al. (2014) Correlation between superoxide dismutase 1 and 2 polymorphisms and susceptibility to oral squamous cell carcinoma. *Exp Ther Med* 7: 171–178. https://doi.org/10.3892/etm.2013.1375

41. Gitik M, Srivastava V, Hodgkinson CA, et al. (2016) Association of superoxide dismutase 2 (SOD2) genotype with gray matter volume shrinkage in chronic alcohol users: replication and further evaluation of an addiction gene panel. *Int J Neuropsychoph* 19. https://doi.org/10.1093/ijnp/pyw033

42. Boroumand F, Mahmoudinasab H, Saadat M (2018) Association of the SOD2 (rs2758339 and rs5746136) polymorphisms with the risk of heroin dependency and the SOD2 expression levels. *Gene* 649: 27–31. https://doi.org/10.1016/j.gene.2018.01.074

43. Mahmoudinasab H, Sanie-Jahromi F, Saadat M (2016) Effects of extremely low-frequency electromagnetic field on expression levels of some antioxidant genes in human MCF-7 cells. *Mol Biol Res Commun* 5: 77–85.

Instructions for Authors

Essentials for Publishing in this Journal

1   Submitted articles should not have been previously published or be currently under consideration for publication elsewhere.

2   Conference papers may only be submitted if the paper has been completely re-written (taken to mean more than 50%) and the author has cleared any necessary permission with the copyright owner if it has been previously copyrighted.

3   All our articles are refereed through a double-blind process.

4   All authors must declare they have read and agreed to the content of the submitted article and must sign a declaration correspond to the originality of the article.

Submission Process

All articles for this journal must be submitted using our online submissions system. http://enrichedpub.com/ . Please use the Submit Your Article link in the Author Service area.

Manuscript Guidelines

The instructions to authors about the article preparation for publication in the Manuscripts are submitted online, through the e-Ur (Electronic editing) system, developed by **Enriched Publications Pvt. Ltd**. The article should contain the abstract with keywords, introduction, body, conclusion, references and the summary in English language (without heading and subheading enumeration). The article length should not exceed 16 pages of A4 paper format.

Title

The title should be informative. It is in both Journal's and author's best interest to use terms suitable. For indexing and word search. If there are no such terms in the title, the author is strongly advised to add a subtitle. The title should be given in English as well. The titles precede the abstract and the summary in an appropriate language.

Letterhead Title

The letterhead title is given at a top of each page for easier identification of article copies in an Electronic form in particular. It contains the author's surname and first name initial .article title, journal title and collation (year, volume, and issue, first and last page). The journal and article titles can be given in a shortened form.

Author's Name

Full name(s) of author(s) should be used. It is advisable to give the middle initial. Names are given in their original form.

Contact Details

The postal address or the e-mail address of the author (usually of the first one if there are more Authors) is given in the footnote at the bottom of the first page.

Type of Articles

Classification of articles is a duty of the editorial staff and is of special importance. Referees and the members of the editorial staff, or section editors, can propose a category, but the editor-in-chief has the sole responsibility for their classification. Journal articles are classified as follows:

Scientific articles:

1. Original scientific paper (giving the previously unpublished results of the author's own research based on management methods).

2. Survey paper (giving an original, detailed and critical view of a research problem or an area to which the author has made a contribution visible through his self-citation);

3. Short or preliminary communication (original management paper of full format but of a smaller extent or of a preliminary character);

4. Scientific critique or forum (discussion on a particular scientific topic, based exclusively on management argumentation) and commentaries. Exceptionally, in particular areas, a scientific paper in the Journal can be in a form of a monograph or a critical edition of scientific data (historical, archival, lexicographic, bibliographic, data survey, etc.) which were unknown or hardly accessible for scientific research.

Professional articles:

1. Professional paper (contribution offering experience useful for improvement of professional practice but not necessarily based on scientific methods);

2. Informative contribution (editorial, commentary, etc.);

3. Review (of a book, software, case study, scientific event, etc.)

Language

The article should be in English. The grammar and style of the article should be of good quality. The systematized text should be without abbreviations (except standard ones). All measurements must be in SI units. The sequence of formulae is denoted in Arabic numerals in parentheses on the right-hand side.

Abstract and Summary

An abstract is a concise informative presentation of the article content for fast and accurate Evaluation of its relevance. It is both in the Editorial Office's and the author's best interest for an abstract to contain terms often used for indexing and article search. The abstract describes the purpose of the study and the methods, outlines the findings and state the conclusions. A 100- to 250-Word abstract should be placed between the title and the keywords with the body text to follow. Besides an abstract are advised to have a summary in English, at the end of the article, after the Reference list. The summary should be structured and long up to 1/10 of the article length (it is more extensive than the abstract).

Keywords

Keywords are terms or phrases showing adequately the article content for indexing and search purposes. They should be allocated heaving in mind widely accepted international sources (index, dictionary or thesaurus), such as the Web of Science keyword list for science in general. The higher their usage frequency is the better. Up to 10 keywords immediately follow the abstract and the summary, in respective languages.

Acknowledgements

The name and the number of the project or programmed within which the article was realized is given in a separate note at the bottom of the first page together with the name of the institution which financially supported the project or programmed.

Tables and Illustrations

All the captions should be in the original language as well as in English, together with the texts in illustrations if possible. Tables are typed in the same style as the text and are denoted by numerals at the top. Photographs and drawings, placed appropriately in the text, should be clear, precise and suitable for reproduction. Drawings should be created in Word or Corel.

Citation in the Text

Citation in the text must be uniform. When citing references in the text, use the reference number set in square brackets from the Reference list at the end of the article.

Footnotes

Footnotes are given at the bottom of the page with the text they refer to. They can contain less relevant details, additional explanations or used sources (e.g. scientific material, manuals). They cannot replace the cited literature.
The article should be accompanied with a cover letter with the information about the author(s): surname, middle initial, first name, and citizen personal number, rank, title, e-mail address, and affiliation address, home address including municipality, phone number in the office and at home (or a mobile phone number). The cover letter should state the type of the article and tell which illustrations are original and which are not.

Address of the Editorial Office:

Enriched Publications Pvt. Ltd.
S-9,IInd FLOOR, MLU POCKET,
MANISH ABHINAV PLAZA-II, ABOVE FEDERAL BANK,
PLOT NO-5, SECTOR -5, DWARKA, NEW DELHI, INDIA-110075,
PHONE: - + (91)-(11)-45525005